Study of Microstructure and Piezoelectric Properties of Synthesized PZT by Commercially Available Precursors

By

Amna Idrees

School of Chemical and Materials Engineering

National University of Sciences and Technology

H-12 Islamabad, Pakistan

October 2023

Study of Microstructure and Piezoelectric Properties of Synthesized PZT by Commercially Available Precursors

Name: Amna Idrees

Reg. No:

00000326839

This thesis is submitted as partial fulfillment of the Requirementsfor the degree of

MS in Nanoscience and Engineering

Supervisor Name: Dr. Mohsin Saleem

School of Chemical and Materials Engineering

National University of Sciences and Technology

H-12 Islamabad, Pakistan

October 2023

THESIS ACCEPTANCE CERTIFICATE

Certified that final copy of MS thesis written by Ms **Amna Idrees** (Regn No 00000326839), of School of Chemical & Materials Engineering (SCME) has been vetted by undersigned, found complete in all respects as per NUST Statues/Regulations, is free of plagiarism, errors, and mistakes and is accepted as partial fulfillment for award of MS degree. It is further certified that necessary amendments as pointed out by GEC members of the scholar have also been incorporated in the said thesis.

Signature: _____

Name of Supervisor: **Dr Mohsin Saleem**

Date: ___07/11/2023___

Signature (HOD): _____

Date: ___08/11/23___

Signature (Dean/Principal): _____

Date: ___8.11.2023___

National University of Sciences &Technology (NUST)

MASTER'S THESIS WORK

hereby recommend that the dissertation prepared under our supervision by

n No & Name: <u>00000326839 Amna Idrees</u>

de: **Study of Microstructure and Piezoelectric Properties of Synthesized PZT by ommercially Available Precursors.**

Presented on: **26 Oct 2023** at: **1400 hrs in SCME (Seminar Hall)**

Be accepted in partial fulfillment of the requirements for the award of Masters of Science degree in **Nanoscience & Engineering.**

Guidance & Examination Committee Members

Name: <u>Dr Muhammad Talha Masood</u>   Signature: _____

Name: <u>Dr Hamid Jabbar</u> (CEME)   Signature: _____

Name: <u>Dr Sofia Javed</u> (Co-Supervisor)   Signature: _____

Supervisor's Name: <u>Dr Mohsin Saleem</u>   Signature: _____

Dated: _30-10-2023_

Head of Department   20/10/23

Date _____

Dean/Principal

Date _____ 6.11.2023

School of Chemical &Materials Engineering (SCME)

Form TH-1
(Must be type written)

National University of Sciences & Technology (NUST)
MASTER'S THESIS WORK
Formulation of Guidance and Examination Committee (GEC)

Amna Idrees

NUST Regn No: __00000326839__

ent: _____SCME_____

Specialization: **MS In Nanoscience & Engineering**

our Completed: ___18___ 24

CGPA: (3.50) 3·38

Work Completed

S/No	Code	Title	Core/Elective	CH	Grade
1	MSE-856	Nanomaterials and Processing	Core	3	A
2	MSE-854	Characterization of Materials	Core	3	B
3	NSE-813	Essentials of Nanoscience and Engineering	Core	3	A
4	NSE-845	Nanolithography and Device Fabrication	Elective	3	B
5	MSE-872	Composite Materials	Elective	3	B+
6	NSE-812	Environmental Nanotechnology	Elective	3	B+
7	RM-898	Research Methodology	Additional	2	Q
8	NSE-842	Nano Materials for Energy Application	Elective	3	B
9	NSE-843	Nano Technology & Photovoltaics	"	3	B

Exam By
12/10?

Date: 5TH October,2021

Student's Signature _____

Thesis Committee

1. Name: **Dr. Mohsin Saleem (Supervisor)**   Signature: _____
   Department: **SCME, NUST**
2. Name: **Dr Sofia Javed Co-Supervisor**   Signature: _____
   Department: **SCME, NUST**
3. Name: **Dr Hamid Jabbar**   Signature: _____
   Department: **CEME, NUST**
4. Name: **Dr Muhammad Talha Masood**   Signature: _____
   Department: **SCME, NUST**
   (External)
6. Name: _____   Signature: _____
   Department: _____

Date: _25/10/2021_

Signature of Head of Department: _____

APPROVAL

Date: _25-10-2021_

_____
Dean/Principal

Dedications

This study is sincerely dedicated to my beloved family, who have been my source of inspiration and gave me strength when I thought of giving up, they continually provide their moral, spiritual, emotional, and financial support.

Acknowledgments

Abstract

Since the discovery of ferroelectric ceramics, materials, and methods have been continuously improved, leading to a sizable number of industrial and commercial applications. Due to its superior dielectric, ferroelectric, and piezoelectric characteristics, the solid solution of $Pb(Zr_{1-X}, Ti_X)O_3$, also known as lead zirconate titanate (PZT), has received much research over the past 40 years. The compositions discovered close to the morphotropic phase boundary (MPB) between the tetragonal and rhombohedral have the greatest piezoelectric coefficients of $PZT.PbO$, TiO_2, and ZrO_2 often interact in a solid-state process to create PZT. The majority of sources concur that the solid state reaction typically starts with the creation of a highly tetragonal lead titanate solid solution, in which the remaining PbO and ZrO_2 are dissolved to form $Pb(_{Zr1-X}Ti_X)O_3$. This work focuses on the synthesis of piezoelectric material using lead from spent lead acid batteries with better dielectric constant and high piezoelectric coefficient. Used lead acid battery powder, which is more affordable than the previous precursor $(Pb(C_6H_6O_7)H_2O)$, was used to create lead zirconate titanate ceramics with the morphological boundary phase PMP composition $Pb(Zr_{0.52}TiO_{0.48})O_3$ or PZT. The products were examined by RAMAN, FTIR, DSC, SEM and XRD, and TGA. The lead powder was calcined to produce orthorhombic β-PbO yellow in colour. Later, this β-PbO was employed to synthesise $Pb(Zr_{0.52}TiO_{0.48})O_3$ as a precursor. PZT ceramics sintered at 1200°C for 6h hours revealed a piezoelectric coefficient of d_{33} 307(pC/N), a Q_m factor of 2081.80, and a dielectric constant of 1597 at 8.5 Hz.

Table of Content

List of Figures

Chapter 1:

Introduction

The previous decades have seen a revolution in consumer electronics. Because of their distinctive electromechanical capabilities, piezoelectric materials are very sought-after. Mechanical stress can be changed into a signal that is electrical using piezoelectric materials, and electrical energy may be changed into mechanical stress.

An applied electric field may create strain in certain materials, or alternatively, an external mechanical load may polarise the material. This phenomenon has further applications in electrical sensors and particular actuators. Applications include electronic fuel injectors, car airbag sensors, accelerometers, gyroscopes, magnetometers, camera zooming, and focusing., in figure 1 [1, 5, 6].
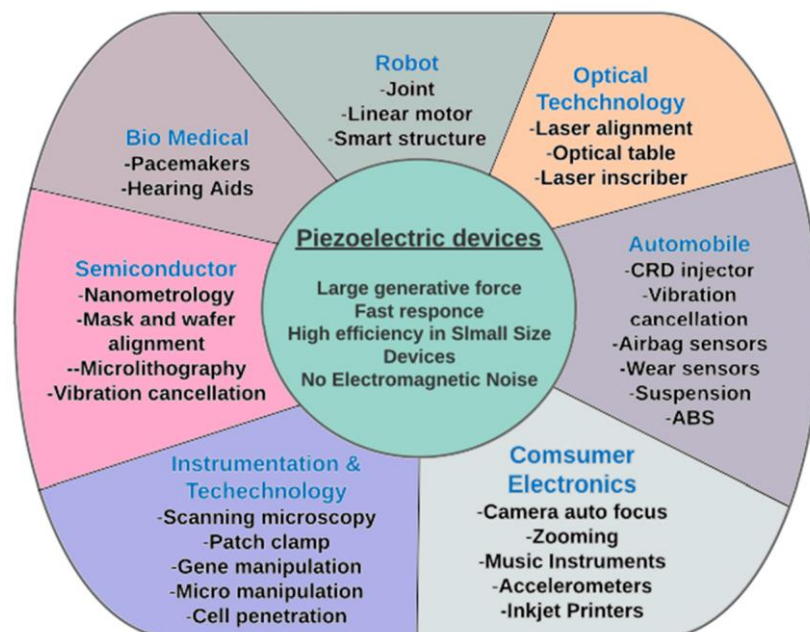
Figure 1 Applications of Piezoelectric materials.

Lead-based ceramics with exceptional ferroelectric and dielectric characteristics, such as lead-zirconate-titanate (PZT), have dominated the piezoelectric industry.
Lead's extreme toxicity to the environment and human health is the fundamental issue with employing lead-based piezoelectric materials. When lead is synthesized, used incorrectly, or recycled, lead can leak into the environment. In extreme circumstances of significant lead

exposure, lead poisoning can result in major health problems such organ failure. The European Union established regulatory bodies for "Waste Electrical and Electronic Equipment" (WEEE) and "Restriction of the use of certain Hazardous Substances in Electrical and Electronic Equipment" (RoHS) in 2003 to limit the use and interaction of Lead and other similar toxic matter from everyday equipment [1]. The fundamental goal of WEEE is to govern the recycling
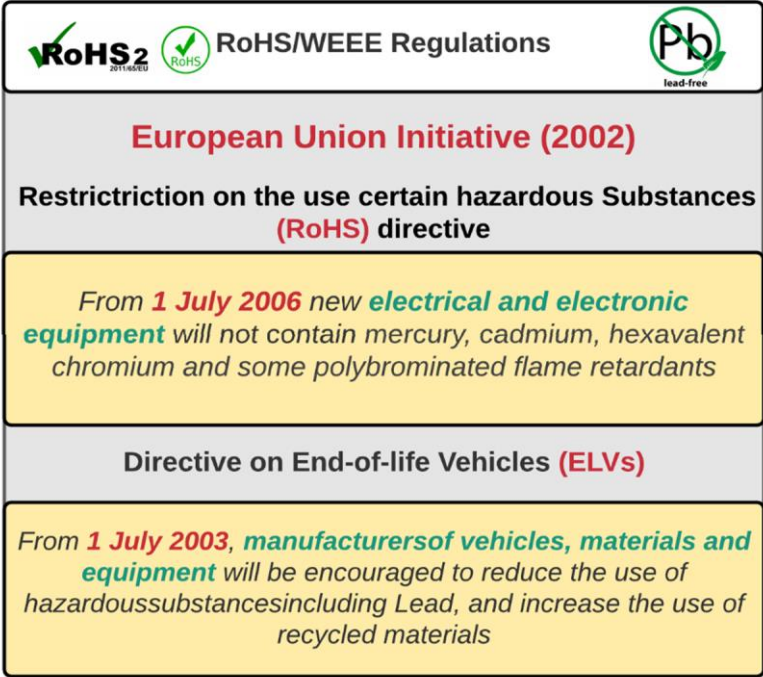
Figure 2 WEEE and RoHS directive
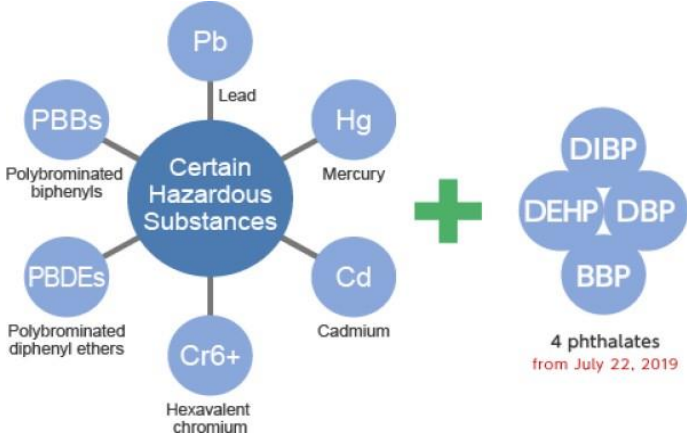
Figure 3 Harmful materials regulated by RoHS.

and disposal of hazardous materials-containing equipment. At the same time, RoHS assures that the process is done without jeopardizing people's health and safety, as well as being suitable for the environment. Figure 2 depicts the regulated dangerous elements, including lead [7].

RoHS enacted the legislation in June 2006, indicating that the maximum allowable level for reported hazardous compounds in consumer items is 0.1 wt.%, with cadmium having a

significantly lower allowed limit of 0.01 wt.%. The sole exemption now is for lead-based piezoelectric devices. Because of their weak electromechanical characteristics, known lead-free piezoceramic materials cannot completely replace lead-containing materials. The exemption for piezoelectric components is constantly reviewed and open to change considering new findings. The exemption further states that those materials in new applications may only become available on the market if the overall environmental and health advantages of the replaced material do not outweigh the present ones. [5, 7]

Prior to the directive, research mostly concentrated on PZT materials systems with improved local lead for features such as enhanced Curie point Tc, polarisation, and so on for actuators and sensors.

1.1 Discovery of Piezoelectric Effect:

In 1880, Pierre and Jacques Curie discovered the piezoelectric phenomenon [8]. Topaz, quartz, Rochelle salt, and other naturally occurring minerals exhibit the piezoelectric effect. Marie Curie's thesis adviser, Gabriel Lipmann, eventually developed and demonstrated the opposite piezoelectric effect.

1.2 Ferroelectrics:

Ferroelectric materials are those that show spontaneous polarization. These materials can create polarization, which can be altered by changing the direction of the applied electric field. At high temperatures, these materials display a temperature-dependent paraelectric phase. It is a temperature sensitive characteristic. The Curie temperature Tc is the level of temperature that
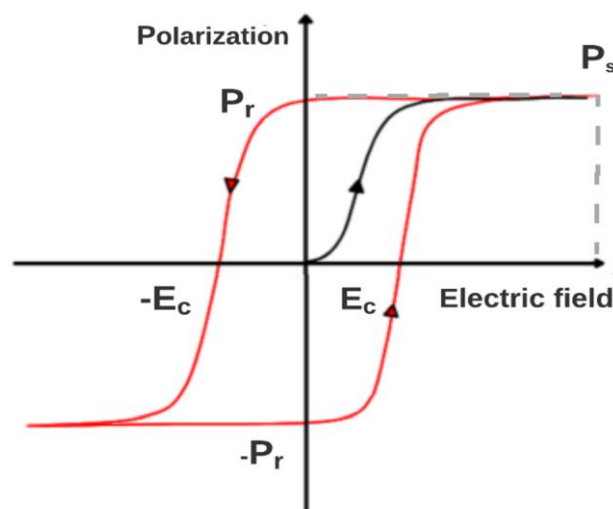
Figure 4 Hysteresis loop for normal ferroelectrics

exists where the ferroelectric characteristics of the material cease. The material is no more ferroelectric at that temperature. Figure 4 depicts an analysis of ferroelectric characteristics using polarization vs. electric field loops. Polarization hysteresis loops are related to ferromagnetic hysteresis loops in such a way that the polarization P in ferroelectrics corresponds to the magnetization M in ferromagnets. As illustrated in Figure 4, the electric field E correlates to the magnetic field H, and the electric displacement D relates to the flux density B.

Piezoelectric characteristics are present in all ferroelectric materials. The switch over manners of ferroelectrics is also employed in a variety of transducer and actuator applications, such as $PbZr_xTi_{1-x}O_3$.

1.3 Piezoelectricity:

In the non-centrosymmetric unit cell, the piezoelectric effect is connected to charge symmetry. In other words, it is caused by the lack of charge symmetry at the unit cell's center. They are classified into 21 crystal classes that lack a center of symmetry. Except for one, all these exhibit piezoelectric characteristics. Commercially accessible piezoelectric materials typically feature perovskite structures made up of solid solutions, such as $PbTiO_3$. $PbTiO_3$ [9] exhibits a non-piezoelectric cubic unit cell above the Tc (curie point). However, spontaneous polarization occurs when the material has been cooled lower than its Tc (curie point). This is due to the structure changing from cubic to tetragonal [10].

1.4 Piezoelectric Materials:
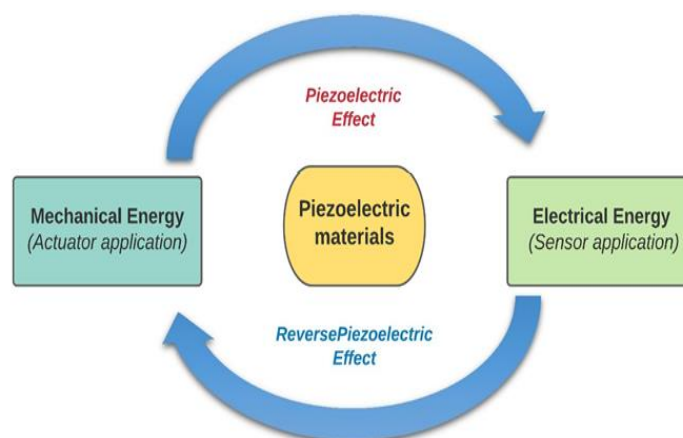
Figure 5 Piezoelectric mechanism and its application

Piezoelectric materials have the capacity to change either mechanical stress or electrical signal

into the other. In other words, they are electromechanically linked. These materials are widely used in engineering services and consumer goods, where they may transform mechanical stress into electrical signals, as in sensors, or electrical power into mechanical displacement, as in actuators.

1.5 Piezoelectric Effects and Related Equations:

In a nutshell, piezoelectricity is defined as a periodic electromechanical connection between mechanical and electrical states. The coefficient for such a linearly proportional connection is described as the piezoelectric coefficient d, which is a third-rank tensor linking the third-rank tensor or vector (electric displacement or field) with the second-rank tensor (stress or strain). The piezoelectric equations can therefore be represented in this way. as (i, j, k = 1, 2, 3).

$$D_k = d_{kij}T_{ij}$$

$$S_{ij} = d_{kij}^* E_k$$

where Di is the electric displacement component (C/m2), Ei is the electric field component (V/m), Sij is the strain component, Tij is the stress component (N/m2), and dkij or dkij* is the piezoelectric charge component or strain constant. It must be well-known that the piezoelectric constant subscripts are frequently expressed via the reduced Voigt matrix notation dkm, where k denotes the portion of electric displacement D or field E in the Cartesian reference frame (x1, x2, x3) and the index m = 1...6 denotes mechanical stress or strain. In this scenario, m = 1, 2, and 3 represent the normal stresses along the x_1, x_2, and x_3 axes, respectively, whereas m = 4, 5, and 6 represent the shear stresses T_{23}, T_{13}, and T_{12}, accordingly. Both d and d* are known as the

Symbol	Name	Definition
d	Piezoelectric charge coefficient or piezoelectric strain coefficient	$d_{ij} = \left(\dfrac{\partial D_i}{\partial T_j}\right)_E = \left(\dfrac{\partial S_j}{\partial E_i}\right)_T$
g	Piezoelectric voltage coefficient (voltage output constant)	$g_{ij} = -\left(\dfrac{\partial E_i}{\partial T_j}\right)_D = \left(\dfrac{\partial S_j}{\partial D_i}\right)_T$
e	Piezoelectric stress coefficient	$e_{ij} = -\left(\dfrac{\partial T_j}{\partial E_i}\right)_S = \left(\dfrac{\partial D_i}{\partial S_j}\right)_E$
h	Piezoelectric stiffness coefficient	$h_{ij} = -\left(\dfrac{\partial E_i}{\partial S_j}\right)_D - \left(\dfrac{\partial T_j}{\partial D_i}\right)_S$

Figure 6 Piezoelectric constants

piezoelectric constant or coefficient, but they're measured in distinct units: pC/N and pm/V (here,

p stands for 109). Thermodynamic considerations lead to the conclusion that dkm = dkm*, i.e., the coefficients linking the field and strain are equivalent to the ones connecting the stress and polarization.

1.6 Piezoelectric Constants:

1.6.1 Piezoelectric Charge (Strain) Constant:

The connection between the electric charge produced per unit area and an applied mechanical force is expressed by the piezoelectric charge coefficient (C/N). [1]. This constant is most used to assess the quality of a piezoelectric material.

$$d = \frac{\text{Strain developed}}{\text{Applied field}} = \frac{\text{Charge density (open circuit)}}{\text{Applied stress}}$$

The d constant is linked to three essential material characteristics via the subsequent calculation:

$$d = k\sqrt{\varepsilon_0 k^T s^E} \quad (C/N)$$

wherever k represents the electromechanical coupling coefficient, kT the relative dielectric constant at constant stress, and sE the elastic compliance (10 m/N) at constant electrical field. Around exist double critical d constants:

$$d_{31} = k_{31}\sqrt{\varepsilon_0 k_3^T s_{11}^E} \quad (C/N)$$

$$d_{33} = k_{33}\sqrt{\varepsilon_0 k_3^T s_{11}^E} \quad (C/N)$$

It is crucial to remember that large d constants, which are frequently attained in motional transducer systems, correlate to sizable mechanical displacements. On the other hand, the coefficient may be considered as connecting the charge that has collected on the electrodes to the applied mechanical stress. when the force is applied in three directions (perpendicular to the polarization axis) and imprinted on the precise surface where the charge is gathered, d_{33} is applied. When the charge is taken in from the same surface as d_{33}, but the force exerted is at a 90-degree angle to the polarisation axis, d_{31} applies. They are well known for possessing the following empirical relationship.

$$d_{33} \approx -2.5 \cdot d_{31}$$

1.6.2 Piezoelectric Voltage Coefficient (G-constant):

The piezoelectric voltage coefficient, commonly referred to as the voltage output constant, is a measure of the relationship between the mechanical stress and electric field created during a piezoelectric process. voltage-meter/Newton (Vm/N).

$$g = \frac{\text{Strain Developed}}{\text{Applied Charge Density}} = \frac{\text{Field Developed}}{\text{Applied Mechanical Stress}}$$

The g-constants are derived as of the equation using the piezoelectric charge (strain) constant (d) and relative permittivity (ε) from the equation:

$$g = \frac{d}{\varepsilon} \ (\text{Vm/N})$$

The g constant can be classified as g_{33}, g_{31}, or g_{15} varying on the nature of comparative paths, corresponding to d_{33}, d_{31}, or d_{15}, respectively.

1.6.3 Piezoelectric Coupling Coefficient:

The ratio of mechanical energy collected in response to an electrical input or vice versa is known as the piezoelectric coupling coefficient (also known as the electromechanical coupling coefficient). Additionally, it relates to the percentage of electrical energy that may be changed into mechanical energy and conversely. Consequently, the following equation may be used to represent the piezoelectric coupling coefficient:

$$X = \frac{\sqrt{\text{Mechanical Energy Stored}}}{\sqrt{\text{Electrical Energy Applied}}} = \frac{\sqrt{\text{Electrical Energy Applied}}}{\sqrt{\text{Mechanical Energy Stored}}}$$

The coupling factor may be calculated using the measured resonance and anti-resonance frequencies of a piezoelectric element, depending on the vibration mode at which the element is stimulated. For vibration in a circle-shaped disc across the radius and thickness directions, respectively, the most frequently encountered linking factors are k_p and k_t. The helpful variable the following formula, known as k_{eff}, is frequently used to determine the effective coupling coefficient of a resonator of any shape, either at any overtone modes or at its fundamental resonance.:

$$k_{eff}^2 = 1 - \left(\frac{f_r}{f_a}\right)^2$$

where f_r and f_a represents resonating frequency and anti-resonating frequency, respectively. The following formulae may be used to compute the coupling coefficients for the different vibration modes:

$$\frac{k_p^2}{1 - k_p^2} = \frac{(1 - \sigma^E)J_1[\ \eta_1(1 + \frac{\Delta F}{F_r})] - \ \eta_1(1 + \frac{\Delta F}{F_r})J_0[\ \eta_1(1 + \frac{\Delta F}{r})]}{(1 - \sigma^E)J_1[\ \eta_1(1 + \frac{\Delta F}{F_r})]}$$

Where,

J   Bessel function of the first kind and zero order.

J_1 Bessel function of the first kind and first order

σ^E Poisson's ratio

η_1 Lowest positive root of $(1+\sigma^E)\cdot J1\eta = \eta J_0(\eta)$

F_r Resonance frequency (Hz)

F_a Anti-resonance frequency (Hz)

$\Delta F = F_a - F_r$ (Hz)

For PZT ceramics, the following simplified equations apply if $\sigma^E = 0.31$ and $\eta_1 = 2.05$:

$$k_{33}^2 = \frac{\frac{\pi}{2}}{1 + \frac{\Delta F}{F_r}} \tan \frac{\frac{\pi}{2}\frac{\Delta F}{F_r}}{1 + \frac{\Delta F}{F_r}}$$

$$\frac{k_{31}^2}{1 - k_{31}^2} = \frac{\pi}{2}\left(1 + \frac{\Delta F}{F_r}\right)\tan\frac{\pi}{2}\frac{\Delta F}{F_r}$$

1.6.4 Mechanical Quality Factor:

The mechanical Q_m (also known as Q), which is correlated with the sharpness of the resonance frequency, is the proportion of reactance to resistance in the circuit that represents a piezoelectric resonator in series. The mechanical Q_m may be calculated using the following equation.

$$Q_m = \frac{f_r}{f_2 - f_1}$$

The frequencies f_1 and f_2 are located at−3 dB of the maximum access, Where f_r is the resonance frequency. The electromechanical coupling factor k and the mechanical Q_m are connected by the following equation:

$$Q_m = \frac{1}{2\pi F_r Z_m C_0}\left(\frac{F_a^2}{F_a^2 F_r^2}\right)$$

Where,

F_r Resonance frequency (Hz)

F_a Anti-resonance frequency (Hz)

Z_m Impedance at F_r (ohm)

C_0 Static capacitance (Farad)

1.7 Morphotropic phase boundaries MPB:

When many phases coexist near the morphotropic phase boundary, materials often display their piezoelectric capabilities. The phase boundary caused by composition is shown at vertical MPB in PZT (Pb (Zr, Ti) O_3). At the rhombohedral/tetragonal phase border, where titanium Ti is present in a 0.48 molar ratio, it has been shown that a significant piezoelectric effect is present in the solid solution. Additionally modifying the MPB composition with chemical dopants yields ceramics with high piezoelectric characteristics [11-13]. In lead-free ceramics like $(Bi_{0.5} Na_{0.5})$ TiO_3, $(Bi_{0.5} K_{0.5})$ TiO_3, $(Bi_{0.5} Na_{0.5})$ TiO_3, $BaTiO_3$, etc., the MPB is also seen [16]. These materials' composition at MPB exhibits good electromechanical characteristics, making them strong candidates for use as free-of-lead piezoelectric materials.

1.8 Polarization and Strain Vs. Electric field:

The most important factor for comprehending and designing ferroelectric materials is polarization hysteresis curves. When an electric field is applied across an unpolarized ferroelectric material below the Curie point T_c, the dipoles start to align in the direction of the applied field. The developing electric field will ultimately cause the polarization to stop increasing.

All the dipoles are arranged according to the applied field, hence the material's saturation polarization value, or Ps, is at its highest. Polarization will not be zero, but rather a precise number represented by remnant polarization Pr, if the applied field is decreased to zero. All of the dipoles do not revert to their initial orientation due to the extremely high remnant degrees of alignment of the dipoles.

The material's polarization becomes zero if the applied field is reversed. Coercive field Ec is the applied field at this time, as seen in figure 8. When the applied field is increased in the opposite direction, the polarization advances until it reaches the saturation polarization, or -Ps; when it is decreased to zero, it reaches the residual polarization, or -Pr. As seen in Figure 7, as the applied field is increased further, the polarization decreases to zero and finally returns to Ps.

As illustrated in Figure 7, the material experiences strain because of the applied electric field,
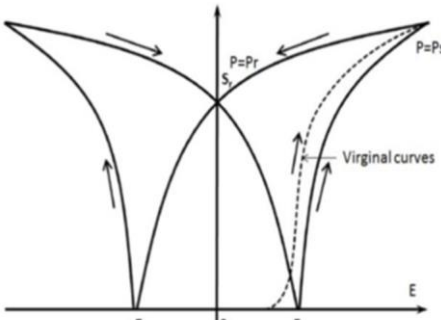
Figure 8 Butterfly strain hysteresis loop

creating the butterfly strain hysteresis loop. It proves that the polarization-induced hysteresis effect is a result of the applied electric field's alteration of strain, which affects the material. The domain shifting does not experience a strain in the area of low electric field. The strain grows
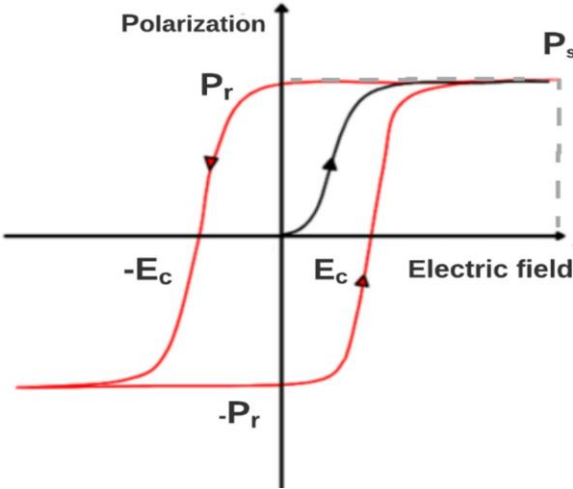
Figure 7 P-E hysteresis loop

quickly when the applied field is increased. When an electric field comes close to the coercive field Ec approaching the maximum intensity at Ps saturation polarization, more domains begin to flip. Even after the applied field is removed, the strain remains high since none of the domains revert to their initial condition. The strain is eliminated, though, if the electric field is raised to a coercive field E_c in the opposite direction. A strain in that direction grows with further growth in the field.

1.9 Actuators:

Devices called piezoelectric actuators use the piezoelectric phenomenon to change electrical power into mechanical motion or the other way around. When subjected to an applied electric field, certain materials, such quartz or ceramics, display the piezoelectric effect, which causes them to alter in dimension. With respect to the polarity of the electrical field, the material will alter in length, breadth, or thickness [14]. This dimension shift causes the material to move mechanically, which may be used to drive action in a system with mechanical components.

By changing the applied voltage, a piezoelectric actuator's motion may be accurately controlled. This makes it possible for accurate orientation and motion control across a variety of applications. Fast reaction times typically in the microsecond range and great resolution on the order of nanometers are two advantages of piezoelectric actuators. They can create strong forces relative to their size and have an elevated force-to-weight ratio.

Scientific instruments, medical equipment, and precision manufacturing all employ piezoelectric actuators extensively. For instance, they are employed in precision manufacturing to precisely regulate the location of machine parts. They are utilized in surgical tools and ultrasonic imaging in medical equipment. They are utilized in telescopes and scanning probe microscopes, both of which are scientific devices.

Overall, due to their high accuracy, quick reaction times, and ability to function in challenging settings, piezoelectric actuators are a flexible and well-liked alternative for precise control and actuation in a wide range of applications.

1.10 Sensors:

Piezoelectric sensors are one form of sensor that takes use of the piezoelectric effect, which is a capability of some materials to create an electric charge in response to specific mechanical stress or pressure. These sensors, which generally include a piezoelectric crystal or material positioned between two electrodes, produce an electrical charge that may be recorded and investigated when a force or pressure is applied. Piezoelectric sensors are often employed in a wide range of products, including pressure sensors, accelerometers, and sound sensors.

Transducers, commonly referred to as active sensors, work using a transmitter-receiver system. To maximise efficiency, the transmitter runs at its resonance frequency and regularly emits

ultrasonic signals. After receiving a signal, the receiver produces an electrical impulse. To calculate distance or depth, the delay is examined. Ultrasonic sensors and level sensors are two examples of this. When a system sends and receives signals, it is referred to as a transducer. It is considerably easier to use passive piezo sensors. When a signal is provided, these specially designed piezo ceramics start to produce electricity; otherwise, they remain dormant. To maximise their detecting range, passive piezo sensors frequently function below their resonance frequency. Accelerometers and touch switches are often used.

In various environments and applications, trustworthy piezoelectric products like piezoelectric sensors are used. Piezoelectric sensors naturally possess a high degree of elasticity that is equivalent to that of certain metals. This keeps reaction times high while enabling a very linear relationship among input and output across a broad range. Most non-piezo sensors are unable to reproduce this degree of response. Piezoelectric sensors are extremely adaptable and can tolerate a variety of environmental extremes, which would ordinarily contaminate sensory data, including extreme temperatures (up to their Curie point), magnetic fields, and radiation. Due to their extremely durable structure, they are the perfect sensor for harsh settings where non-piezo sensors may occasionally malfunction.

Chapter 2:

Literature Review

The phenomenon of piezoelectricity, in which the application of stress causes the material to develop an electric polarization, is visible in non-centrosymmetric crystals. (i.e., charge). On the other hand, the increase of an induced strain is inversely proportional to the applied electric field. The opposite effect is the term used to describe the latter phenomenon, which is also employed in actuation. The former, sometimes referred to as the direct effect, is used to find changes in force, acceleration, and dynamic pressure (due to shock or vibration). [15]

2.1 Lead Free Piezoelectric Materials:

The presence of MPBs is desirable when looking for new complex systems with possibly desirable electromechanical properties, and it must be considered that the stability of the properties versus time, temperature, or pressure is also linked to the phase transition(s) temperature(s) of the material. For instance, materials based on BaTiO3 have Curie temperatures that are too low for most applications but having potentially outstanding electromechanical characteristics. [15]

Potassium sodium niobate ((K,Na)NbO$_3$, KNN), barium titanate (BaTiO$_3$, BT), bismuth sodium titanate ((Bi,Na)TiO$_3$, BNT), and bismuth ferrite (BiFeO$_3$, BFO) are the major components of lead-free piezoelectric ceramics. Due to health and safety concerns, lead-free piezoelectric ceramic development and commercialization have garnered increasing interest since the early
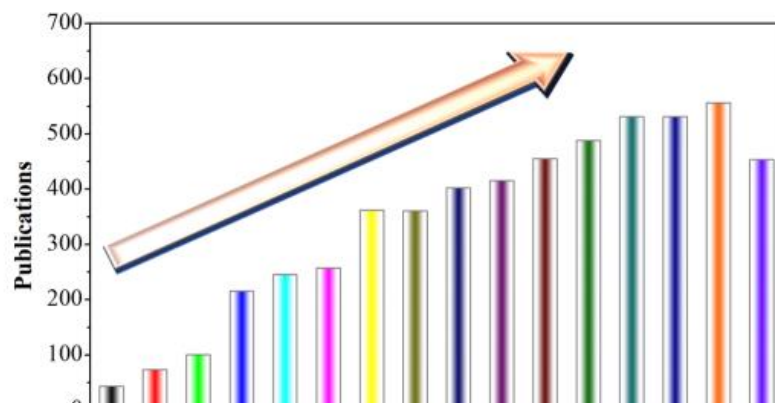
Figure 9 Published papers of lead-free piezoelectric materials from 2004 to 2019 years with keywords including lead-free and piezoelectric ceramics, all data from Web of Science.

2000s. A technical advance in electrical devices was made possible, for instance, by the discovery that the successful fabrication of phase boundaries increased their piezoelectric coefficients in lead-free piezoelectric ceramics. [16, 17]

These ceramics' overall performance in terms of electrical properties has to be enhanced. High Qm and high d33 for "hard" lead-free piezoelectric are challenging to achieve. For the purpose of directing the creation of "hard" lead-free piezoelectric, the related physical mechanisms must be exposed. Increasing density is crucial for energy storage. These lead-free piezoelectric's production procedures, such as multilayer and 3-D printing processes, as well as other characteristics, such as mechanical behaviour, need be considered along with to the electrical parameters. [17]

2.2 Lead based Piezoelectric Materials:

The majority of lead-free piezoelectric materials contain temperature-dependent phase borders, also known as the "morphotropic phase boundary (MPB)," which results in inadequate piezoelectric capabilities, causing the fabrication of lead-free piezoelectric materials challenging. To achieve high performance and stability, it is still essential to acquire the true MPB; at the very least, the electrical characteristics' temperature stability has to be increased.

Due to their superior piezoelectric capabilities, lead oxide based ferroelectrics, namely lead zirconate titanate $(Pb(Zr, Ti)O_3)$ or PZT, are the most often utilised compounds for piezoelectric actuators, sensors, and transducers [18]. Due to their superior piezoelectric capabilities, lead oxide based ferroelectrics, exemplified as lead zirconate titanate $(Pb(Zr,Ti)O_3)$ or PZT, are the most frequently utilised compounds for piezoelectric actuators, sensors, and transducers [1]. The existence of a morphotropic phase boundary (MPB) is a notable characteristic of these materials. The compositions around this limit exhibit exceptional electromechanical characteristics. However, there is increasing concern over the reuse and disposal of PZT-containing devices due to lead oxide toxicity, particularly those utilised in consumer goods like vehicles, different smart systems, and sound generators. The fact that lead oxide vaporises while on manufacturing, that lead remains in the environment for a long time, and that lead accumulates in organisms, harming the brain and neurological system, has resulted in a stiffening of laws in many nations. However, the benefits of PZTs' strong piezoelectric characteristics are plain to see. Using PZT in medical imaging, for instance, enables a good signal amplitude that is necessary for an accurate diagnosis, saving many lives in the process.

2.2.1 Lead Titanate (PbTiO₃):

Although pure lead titanate, or PbTiO3, is not currently utilised in industry as a piezoelectric compound, it may be altered or combined with other substances to create solid solutions that have good piezoelectric capabilities. The majority of piezoelectric used in commercial applications today are solid solutions made from lead titanate. The structure and fundamental characteristics of $PbTiO_3$ are discussed in this section. $PbTiO_3$ is a member of the ABO_3 perovskite family. $PbTiO_3$ has a tetragonal space group and is ferroelectric at normal temperature. At 493°C, lead titanate passes through a first-order phase change. It was often believed that this phase transition was a prototypical displacive phase transition [19], however new research suggests that it really shows mixed displacive and order-disorder characteristics. [20].

Although $PbTiO_3$ and barium titanate ($BaTiO_3$), another common ferroelectric perovskite, are isomorphous at ambient temperature, there are several significant distinctions between the two substances. Lead titanate has a much greater tetragonal lattice deformation than $BaTiO_3$. Another distinction is that, upon cooling from the paraelectric cubic phase, $BaTiO_3$ transitions through a series of ferroelectric phases (cubic-tetragonal-orthorhombic-rhombohedral), whereas lead titanate appears to only have cubic and tetragonal ferroelectric phases. [21]

The ions' coordinates [22] in the tetragonal phase of $PbTiO_3$ may be defined as follows, with the
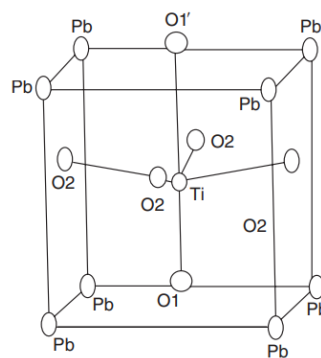
Figure 10 The perovskite structure of lead titanate with distorted oxygen octahedron. The lattice parameters, bond lengths, and angles are determined at room temperature using neutron diffraction of PbTiO3 powder.

Pb ion acting as the coordinate system's origin. $PbTiO_3$ moves in the same direction as Ti and both types of O ions, in contrast to $BaTiO_3$ [23] where O and Ti ions travel in the opposite way. The oxygen octahedron exhibits a large distortion, as demonstrated by neutron single-crystal and neutron powder diffraction refinements of the structure [21, 22], as shown in Fig.10

The literature has extensively investigated the covalent nature of Pb and its function in the ferroelectric and piezoelectric capabilities of Pb-based compounds [24]. The function of Pb in the ferroelectricity of lead-based materials is now clearly understood because to recent advancements in ab-initio calculations, which also explain why $PbTiO_3$ and lead-free perovskites ($BaTiO_3$, $KNbO_3$) have such radically different characteristics. By decreasing short-range repulsions, Cohen has demonstrated that hybridization of the Ti-O link is crucial for ferroelectricity in both $BaTiO_3$ and $PbTiO_3$. The ferroelectric instability vanishes, and the substance becomes cubic if this hybridization is suppressed. According to the calculations, the valence band of $PbTiO_3$ does not hybridise with the 5p states of Ba, but the 2p states of oxygen and the 6s states of lead do. The greater strain in $PbTiO_3$ is thus linked to the lower radius of Pb relative to Ba and the Pb-O bonding interaction. Ti-O interactions are also indirectly impacted by Pb-O hybridization.

There have been very few attempts to systematically explore the dielectric, elastic, and piezoelectric characteristics of this crystal due to the challenges in generating decent single crystals of $PbTiO_3$ that are large enough for testing. The crystals' high conductivity, which may be due to a high concentration of lead vacancies, complicates the experimental research even more. [19]

2.2.2 Lead Zirconate Titanate (PZT):

PbZrO3, or lead zirconate, is not piezoelectric because it is antiferroelectric [19]. There is little use for pure $PbTiO_3$ as a piezoelectric material. The hard blend of these two compositions, $Pb(Zr_{1-x}Ti_x)O_3$ or PZT, surprisingly has exceptional piezoelectric characteristics. PZT is one of the ferroelectrics that has been the subject of the most research because to its extensive usage in
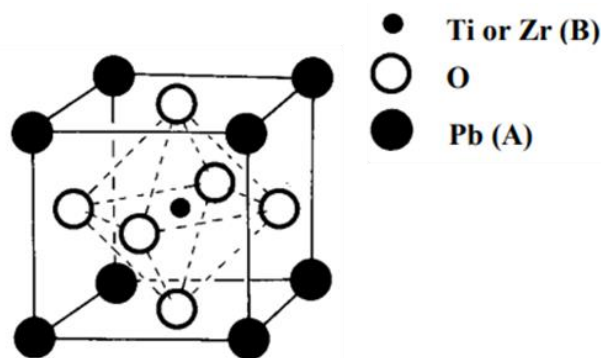
Figure 11 Elementary structural unit of perovskite PZT. The elementary structural unit is a cube. Titanium or zirconium atoms (B) lie at the centre; eight lead atoms (A) occupy the corners and six oxygen atoms (O) are at the surface centres.

business, science, technology, medical, transportation, communications, and information systems. Even yet, there are still many unknowns about the strong piezoelectric response in PZT. The fact that adjustments to this ternary system's composition-temperature phase diagram are continuously being suggested [25], amassing newfound inquiries about the ancestry of the substantial piezoelectric movement in this and associated ferroelectric materials, 50 years after its discovery [4] and numerous in-depth studies [1], may be the best indication of the complexity of PZT.

$PbZrO_{3-(1-x)}$ $PbTiO_3$ has a solid solution phase called PZT. Its molecular structure is $Pb(Zr_{1-x}Ti_x)O_3$. Lead atoms are positioned at the unit cell's corners, oxygen atoms are positioned at the surface's centres, and titanium and zirconium atoms are dispersed across the A-sites of PZT. Fig 11. The oxygen and lead ions' radii are each around 0.14 nm. They come together to form a face-centred, 0.4 nm lattice-parameter cubic array. At the heart of the unit cell are titanium or zirconium ions that are octahedrally coordinated.

2.3 Phase Diagram for $PbTiO_3$-$PbZrO_3$:
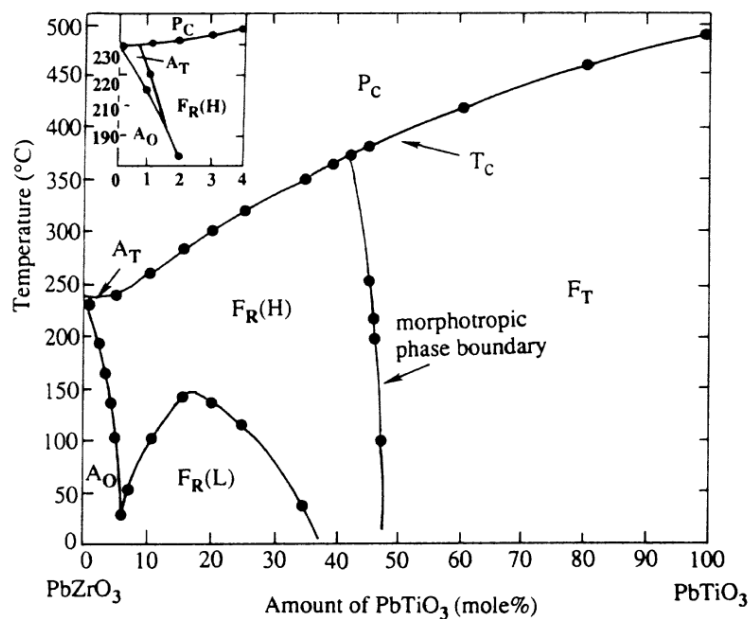
Figure 12 Phase diagram of the PbTiO3-PbZrO3 solid solution [1]

In all ratios, lead zirconate and lead titanate are soluble. In the first phase diagram of $Pb(Zr_{1-x}Ti_x)O_3$, the most noticeable feature of the system is the compositionally induced structural transition from the tetragonal (P4mm) to rhombohedral phase (R3m) at x 0.47 at ambient temperature.by Sawaguchi [26]. Following this investigation, it was quickly shown that

compositions around this phase boundary had a significant piezoelectric response [27]. The "morphotropic phase boundary" (MPB), or border between the tetragonal and rhombohedral (monoclinic) phases, is the most conspicuous aspect of the phase diagram. Jaffe et al. defined the phrase as "an abrupt structural change within a solid solution with variation in composition" [1].

The T_c-line, which denotes the change from the cubic paraelectric phase to the ferroelectric phase, may be seen in Figure 12 as the phase diagram of the PZT solid solution. A morphotropic phase boundary (MPB) separates the regions of ferroelectric phase into two halves: a tetragonal phase region on the Ti-rich side and a rhombohedral phase region on the Zr-rich side. This barrier is located at Zr/Ti = 52/48 when the temperature is ambient. Additionally, the PZT's lattice characteristics quickly alter close to the composition that corresponds to the MPB. Figure 13, the solid solution is an antiferroelectric orthorhombic phase with no discernible piezoelectric action in the area where Zr/Ti falls between 100/0 and 94/6.

The benefits of the PZT solid solution system for use as piezoelectric ceramics are clear from the diagram.

- The cubic symmetry and perovskite structure are present above the Curie temperatures.
- The entire diagram's high Curie temperatures produced stable ferroelectric states across a large, practical temperature range.
- Increased ease of polarisation reorientation during poling is the most frequently cited argument for improved PZT ceramic characteristics at MPB [1] [28]. While polarisation can be oriented along six pseudocubic directions during the tetragonal phase, there are eight potential directions during the rhombohedral phase. Tetragonal and rhombohedral phases coexist at MPB; their free energies are practically degenerate; and external forces, such as a poling field, can influence the phases' transition.. As a result, each grain's polarisation effectively has 14 possible orientations. Greater piezoelectric capabilities are the result of improved poling. In fact, experimental evidence has demonstrated that the MPB region of PZT is where leftover polarisation in PZT reaches its highest.
- The intrinsic property increases in compositions selected close to the border remains throughout a broad temperature range because the MPB is almost vertical on the phase diagram.

The peculiar structure of PZT causes both its dielectric and piezoelectric characteristics to behave abnormally close to the MPB (Fig 13). Both the electromechanical coupling coefficient, a crucial factor in characterizing the piezoelectric characteristics, and the relative permittivity have

a maximum. PZT is a practically valuable piezoelectric material because of its characteristic.
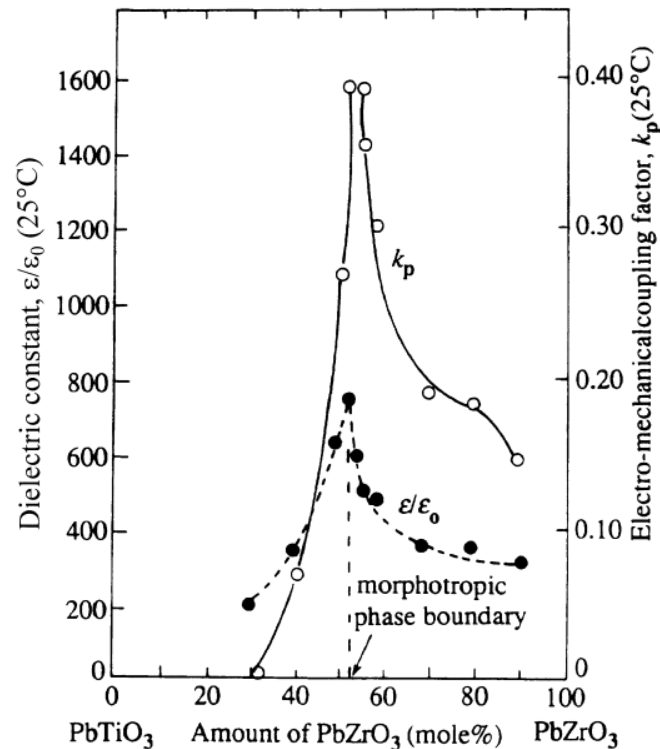
Figure 13 Dielectric and piezoelectric properties of the $PbTiO_3$-$PbZrO_3$ solid solution [1].

2.4 Hard and Soft PZT:

The names "soft" and "hard" PZT ceramics relate to the polarisation and depolarization behaviour as well as the movement of the dipoles or domains. PZT ceramics that are chemically "pure" (or, more accurately, ceramics that are not purposefully doped) have high overall piezoelectric characteristics [27]. However, it was early discovered that the addition of substitutions that create Pb vacancies results in "soft" materials, which are known for their improved resistivity, low ageing, high piezoelectric coefficients, high losses, low mechanical quality factor, and low coercive field. No matter whether donor (higher valence) cations are introduced to the perovskite cell's A or B site, the outcome is qualitatively the same. Nb^{+5} on B site or La^{+3} on A site are typical cations employed. Materials containing oxygen vacancies caused by ionic replacements have lower permittivity, lower resistivity, lower dielectric loss, a higher mechanical quality factor, and harder poling and depoling [1]. They are referred to as "hard" materials, and common acceptor dopants are K^{+1} on the A-site or Fe^{+3} on the B site.

Properties of typical soft and hard PZT materials are shown in figure 14.

					δ

Figure 14 Properties Of soft and hard PZT

High electrical and mechanical loads may be placed on hard PZT materials. They exhibit extremely good stability under these circumstances, with just a small alteration in their attributes. Hard PZT materials are hence appropriate for high-power applications. The moderate permittivity, high coupling ratios, and low losses of hard PZT ceramics are further benefits. These properties enable their continued usage in resonance mode only with minimal intrinsic component warming. These piezo elements are utilised in transformers, sonar technology, medicinal areas, ultrasonic cleaning, ultrasonic processors, and other applications [29, 30]. Large physical property differences between soft and hard groups are mostly caused by contributions to domain wall motion rather than by characteristics of the. But the processes for becoming harder and soften are not well understood. The large difference of the physical properties between soft and hard groups are mainly originated from the contributions of domain wall motion rather than the features of the. However, the mechanisms of hardening and softening are not completely well understood.

2.4.1 P-E curve of Hard and Soft PZT under Compressive stress and loading:

Figures 15 and 16, respectively, depict the polarisation versus electric field (P-E) hysteresis loops of the soft and hard PZT ceramics under various compressive stresses during loading. Firstly, it should be noted that in both soft and hard PZT ceramics, the area of the P-E loops continuously decreases as the compressive stress increases. The P-E loop area represents the energy of polarisation dissipation of a ferroelectric material after one complete cycle of application of an electric field. The volume involved in the switching process when an electric field is applied determines the quantity of energy lost [29]. As a result, the stress-induced domain wall motion suppression is what causes the loop area to shrink with increasing stress [31]. As a result, it is discovered that the polarization dissipation energy drops as the applied stress increases, suggesting that the volume of sample contributing to polarisation reversal diminishes as compressive stress increases.
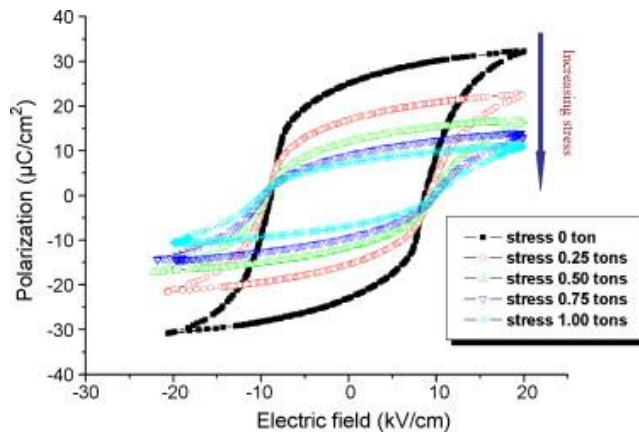
Figure 15 Polarization vs. electric field (P–E) hysteresis loops as a function of compressive stress for Hard PZT ceramic during loading.
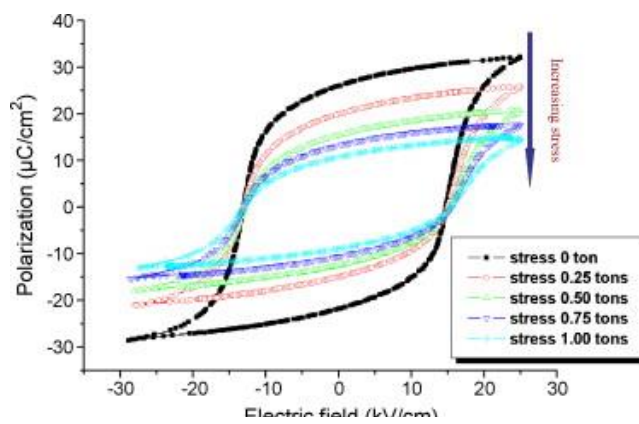
Figure 16 Polarization vs. electric field (P–E) hysteresis loops as a function of compressive stress for soft PZT ceramic during loading.

2.5 Synthesis of PZT Ceramic:

One significant and promising ferroelectric material is lead zirconate titanate (PZT), which is utilised in a variety of electronic devices for data storage, including actuators, sensors, ultrasonic transducers, and electro-optic devices. [29, 32]. Several techniques, including solid-state reaction, semi-wet approach, molecular precursor pathway, oxide co-precipitation sol-gel, and mechanochemical synthesis, have been used to create PZT ceramic powders. both the hydrothermal process and spray drying.

One significant and promising ferroelectric material is lead zirconate titanate (PZT), which is utilised in applications including actuators, sensors, ultrasonic transducers, and electro-optic devices for data storage [29, 32]. PZT ceramic powders have been created using a variety of processes, including spray drying [33], solid state reaction, semi-wet method [34], molecular precursor route [34], hydroxide co-precipitation [35], sol-gel, mechanochemical synthesis [36],

21

and hydrothermal process [37]. PbO, TiO2, and Zr02 are often combined in a solid-state reaction to create PZT (common dry technique). The sequences of this reaction are now well understood, and various studies have provided excellent descriptions of them. Most sources concur that the lead titanate solid solution is typically formed first in the solid-state reaction, followed by the residual PbO and ZrO2, which combine to generate Pb $(Zr_{1-x}Ti_X)$ O3.

2.5.1 PZT powder by conventional method:

Pb($Zr_{0.52}Ti_{0.48}$)O3 was made using the conventional ceramic technique. PbO (massicot, 99.0% purity, Biochem), ZrO2 (baddeleyute, 99.0% purity, Biochem), and TiO2 (60,2% rutile and 39,8% anatase, 99.0% purity) were the initial raw materials utilised. The starting powders were balanced in the requisite stoichiometric ratio for the synthesis of PZT and precursors, and then they were combined in acetone medium for 24 hours using a magnetic stirrer to accomplish homogenization. Following the drying process, the combined powders had been ground in a mortar and pestle for six hours. The powders were compressed into 13 mm-diameter, 2 mm-thick pellets at uni-axial pressure of 750 MPa to facilitate the reactions in solid. On alumina plates, the
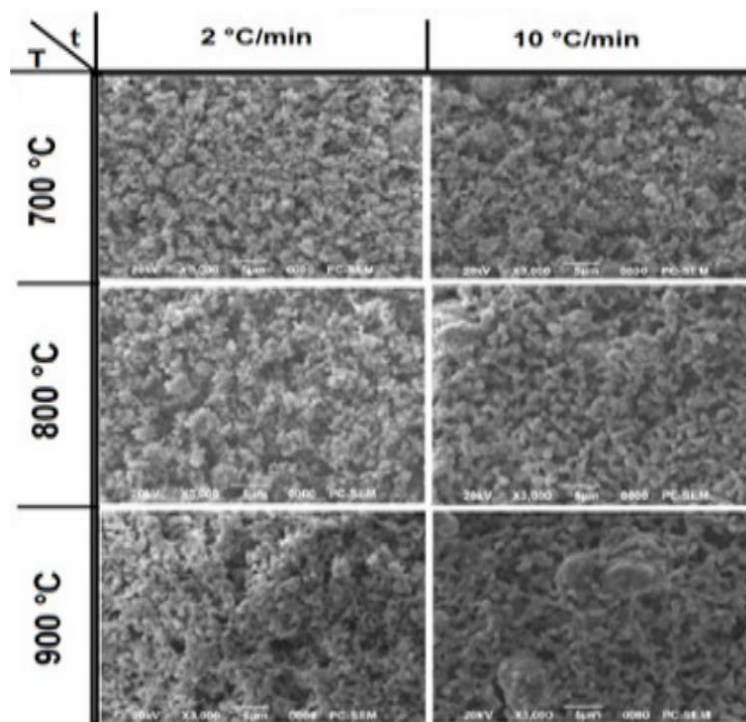
Figure 17 SEM micrographs of powders calcined at different temperatures and for 2h and 6 h of isothermal times [2].

resulting specimens were calcined between 700 and 900 °C. Temperature ramp rates and length (isothermal time) were chosen, and they ranged from 2 to 10°C min1 and 2 to 6 h, respectively.

The results demonstrated that the reaction between the starting materials was incomplete for samples that were calcined at 700 °C with a greater temperature ramp rate (10 °C/min). The result contained residual PbO as well as intermediate solid solutions (PT and PZ). As calcination temperature raised at 800 °C, a single perovskite phase type was seen. When the same powder was heated at higher temperatures for the same isothermal period, the particles produced had less sphericity than those produced at 700°C and rapid heating rates. The raw ingredients were heated for two hours at 800°C using a gradual temperature ramp rate (2∘C/min^{-1}) to produce the regular particles.

2.5.2 Mechanochemical synthesis of PZT powders:

[36] By employing beginning ingredients that were commercially available PbO (Budochemia), ZrO2 (Carlo Erba), and TiO2 (Vetec), all of which were >99.9% pure, PZT powder close to MPB was created. A planetary ball mill was used to further grind the initial oxides in accordance with the chemical composition of the required PZT ceramics. The following were the milling circumstances: Ball-to-powder weight ratio was 40:1, powder amount was 20 g, air atmosphere, basic disc rotation speed was 317 min^{-1}, rotation speed of discs with jars was 396 min^{-1}, and
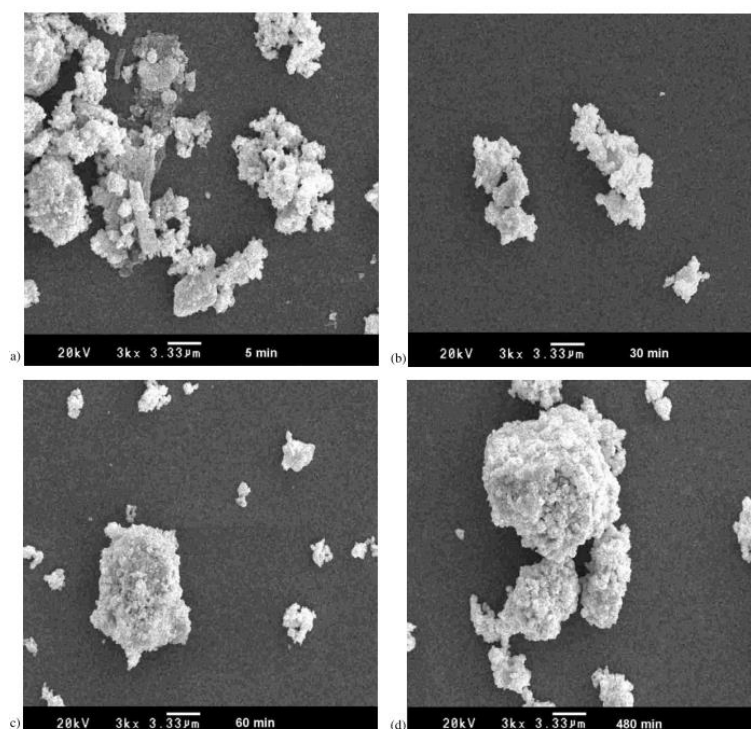
Figure 18 EM of the PZT powder mixtures milled for various times: (a) 5 min, (b) 30 min, (c) 60 min and (d) 480 min.

milling time ranged from 5 to 480 min. The materials used were stainless steel jars (V=500 cm^3) and balls (d=13.4 mm). The first signs of the perovskite phase appeared after 5 minutes of milling.Due to the presence of carbonates and hydroxides, which altered the overall stoichiometry, prepared powders revealed evidence of unreacted ZrO_2. The lowest quantity of unreacted ZrO_2 was found in PZT powder after 120 minutes of mechanochemical treatment.

2.5.3 Molten salt synthesis of PZT powder:

Since the atomic mobility of the reactive species in molten salt is larger than that in solid state reactions, the salt is crucial to the synthesis process [38]. As a result, the response can be finished faster. The salt, or salt mixture, is chosen such that it will: (a) not react with the raw materials or the finished product; (b) be soluble in water so that it may be readily removed by washing; and (c) have a melting point that is comparatively low.

[39] Lead, zirconium, and titanium oxides were used as the starting ingredients in the reported molten salt synthesis method to create PZT powder. As the reaction flow, a 1:1 eutectic molar ratio of NaCl and KCl was utilised. Using ethanol as the carrier, a slurry comprising stoichiometric proportions of the starting ingredients was ball milled for 24 hours with the flux (1:1 by weight). The slurry was mixed, and then the ethanol was removed by drying it at 100 °C for a whole night. The reaction between the starting components was incomplete for shorter durations (30 min). Within the product, residual PbO, ZrO2, and PT were discovered. The particles produced for the same isothermal process at 750°C and rapid rates of heating were less spherical than the similar powder produced at higher temperatures. Excessive particle growth was observed at high temperatures and long reaction times.

2.5.4 PZT nanocrystalline powder by a modified sol–gel process using water as primary solvent source:

The sol-gel procedure is preferred over other methods because to its straightforward setup, stoichiometric control, and comparatively low processing temperature. Alkoxides are frequently used as source ingredients in sol-gel techniques, and organic solvents. However, because transition-metal atoms have a high electropositive character, they are reactive and suffer hydrolysis and condensation quickly when water is introduced. [9]

[40] The sol-gel technique was used to create several perovskites PZT (95/5) powders in the reported process, however water was used as the main solvent for the precursors. Water was used

to dissolve the starting ingredients to create two different 0.15 M solutions. To prevent the development of precipitate, absolute ethanol solution of Ti $(OC_4H_9)_4$ was added to the zirconium oxynitrate aqueous solution using nitric acid. The aqueous solution of Pb_{2+} was then poured into the previously combined solution. As stabilisers, a total of two polyethylene glycols with molecular weights of 6000 and 20,000, in a ratio of 1:1, were utilised. The pH was set to 4 using either urea or diluted ammonia. The acquired sols were kept at room temperature throughout the course of the gelation. After being dried at 120 °C for 24 hours, the gels were crushed in an agate mortar and calcined in air at temperatures between 500 and 700 °C.
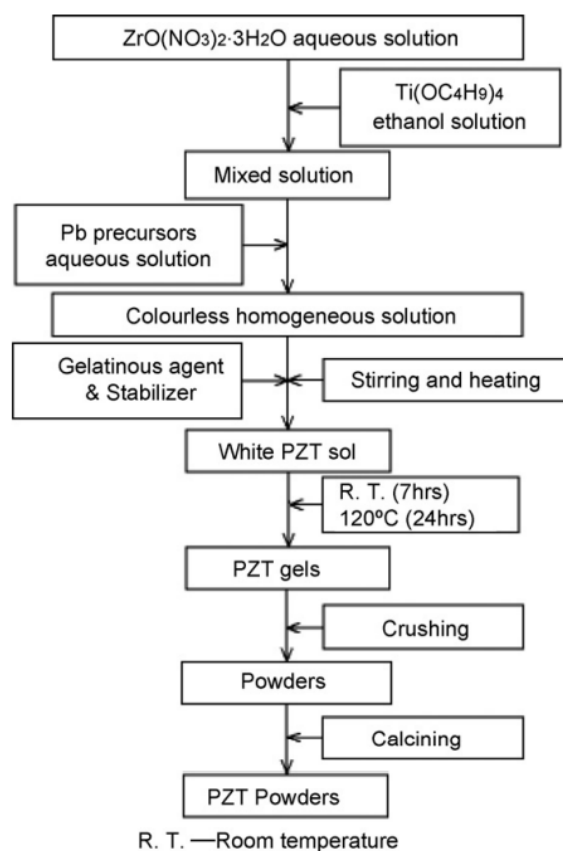
Figure 19 Scheme for the preparation of PZT nanocrystalline powders using water as primary solvent in a modified sol-gel process.

The Pb:Zr:Ti ratio in every sample was 1:0.95:0.05. For the preparation of $Pb(Zr_{0.95}Ti_{0.05})O_3$ nanocrystalline powder, a modified sol-gel technique is created. It is easier to prepare PZT sols when zirconium oxynitrate is employed as the Zr source and water as the major solvent. Other than PZT phases were always present in the powders produced when water was utilised as the solvent. However, adding PEG as a stabiliser can prevent phase segregation. The average size of the PZT powders produced at 700 °C for 2.5 h is 70 nm.

Chapter 3:

Materials and Methods

3.1 Research Objectives:

The goal of this study is to Synthesize PZT ceramic using local precursors.

1. Investigation of microstructure and piezoelectric characteristics of PZT.
2. Characterization of the synthesised material's structural properties.
3. Electromechanical testing of the ceramic material synthesised.
4. Piezoceramic material analysis for piezoelectric applications.

In this study, the following materials are employed to synthesise PZT ceramic.

3.2 Materials:

Following Materials are being used for the synthesis of PZT ceramic in this research.

3.2.1 Lead

Heavier than most other materials and having a greater density. Lead has a low melting point and is pliable and soft. Lead exists in two oxidation states: +4 and +2. The carbon group frequently exhibits the tetravalent state. The divalent state is uncommon in carbon and silicon, minor in germanium, major (but not dominant) in tin, and the more essential of the two oxidation states in lead. In this study, ceramic was used.

Bath drains made of lead pipes decorated with Roman emperor emblems are still in use. Some examples of alloys include pewter and solder. Some forms of fuel (petrol) continue to include tetraethyl lead ($PbEt_4$), however this practise is being phased out owing to environmental concerns.

The lead-acid battery, which is frequently used in vehicle batteries, contains a substantial amount of lead. It is used in projectiles, as a colouring agent in ceramic glazes, and as a wick hazard in certain candles. It serves as an electrode during the electrolysis process and is the typical base metal for organ pipes. It is frequently used to shield the viewer from radiation in the glass of

computer and television screens. Sheets, cables, solders, lead crystal glassware, bullets, bearings, and sport equipment weight are a few further uses.

Atomic number	82
Atomic mass	207.2 g.mol $^{-1}$
Electronegativity (Pauling)	1.8
Density	11.34 g.cm^{-3} at 20°C
Melting point	327 °C
Boiling point	1755 °C

Figure 20 Properties of lead

There are two crystal forms of lead oxide (PbO): red tetragonal (β-PbO) and yellow orthorhombic (β-PbO). While β-PbO is produced at temperatures below 486°C, β-PbO is created at higher temperatures. When lead is thermally oxidised, a PbO layer first develops on the metal surface. This is followed by a solid-state oxidation process, or the diffusion of oxygen vacancies through the PbO layer. The battery business uses leady oxide, a kind of lead powder that has been oxidised to 75-85%.

Both variants of lead oxide, PbO, have very poor electrical conductivity and fascinating semiconducting and photoconducting characteristics. As a result, PbO has industrial uses such as electroradiography , imaging devices, electrophotography, and laser technology. Thin films of lead monoxide are being investigated for use as antireflection coatings in the manufacture of detectors and semiconductor gas sensors.

Lead is a neurotoxic that deposits in bones and soft tissues; it damages the nervous system and causes interference with the action of biological enzymes, resulting in neurological illnesses ranging from behavioural difficulties to brain damage, as well as effects on general health, cardiovascular, and renal systems.

3.2.2 Zirconium

The Arabic name zargon (golden in shade), which is gained from the Persian terms zar (gold) and gun (colour), is whence the word zirconium (Zr) gets its name. [1]. Silver-gray zirconium is an extremely strong, malleable, ductile, and shiny metal. It shares many of titanium's chemical and physical properties. All types of Zr ore contain between 2% and 3% hafnium, with reactor-grade Zr (used in the nuclear industry) having a hafnium level of up to 100 ppm. [5]. Passivation, or coating with an inert layer of oxide, is responsible for its high resistance to corroding, heat, and acid. Zirconium is light weight than steel and has the same hardness as copper. When the metal is finely divided, especially at high temperatures, it may spontaneously fire in the air. Its black powder is regarded as a high-risk fire hazard. Major sources of Zr include deposits in South Africa, the United States, and Australia. It may be found in all biological systems and is often present in high quantities in nature. [5, 41].

Atomic number	40
Atomic mass	91.22 g.mol^{-1}
Electronegativity (Pauling)	1.2
Density	6.49 g.cm-3 at 20°C
Melting point	1852 °C
Boiling point	4400 °C

Figure 21 Properties of zirconium

3.2.3 Titanium:

Titanium appears white-silvery metallic and is a light transition metal. It resists corrosion and is hard and shiny. Titanium is soluble in strong acids but insoluble in water. This metal develops a passive yet protective oxide layer when exposed to high air temperatures, which increases corrosion resistance.

Atomic number	22
Atomic mass	47.90 g.mol^{-1}
Electronegativity (Pauling)	1.5
Density	4.51g.cm^{-3} at 20°C
Melting point	1660 °C
Boiling point	3287 °C

Figure 22 Properties of Titanium

Titanium dioxide (TiO2, also known as titanium (IV) oxide or titania) is an oxide of titanium that occurs naturally. It is known as titanium white, Pigment White 6 (PW6), or CI 77891 when used as a pigment. It is often made from ilmenite, rutile, and anatase. It has several uses, ranging from paint to lotion for sun protection to food colouring. The manner of production is determined on the feedstock.

Titanium dioxide (TiO_2) is by far the most important titanium compound. Titanium dioxide is odourless and a powerful absorbent. Its primary function in powder form is to provide whiteness and opacity. When used as a bleaching and opacifying agent, titanium dioxide gives materials brightness, hardness, and acid resistance.

Due to its distinct characteristics, titanium dioxide is often used and well-known in nanoscience and technology. Titanium dioxide was one of the first materials used in nanotechnology goods. It is questionable whether titanium dioxide nanoparticles are harmful or not. Nanoparticles made of titanium dioxide are used by several industries. Due to its brilliant whiteness, it may be used in products like face powder, coatings, and toothpaste.

3.3 Synthesis Routes for Piezoelectric Ceramics:

Piezoelectric ceramic powders are mainly prepared by following synthesis routes as depicted in schematic figure 23.
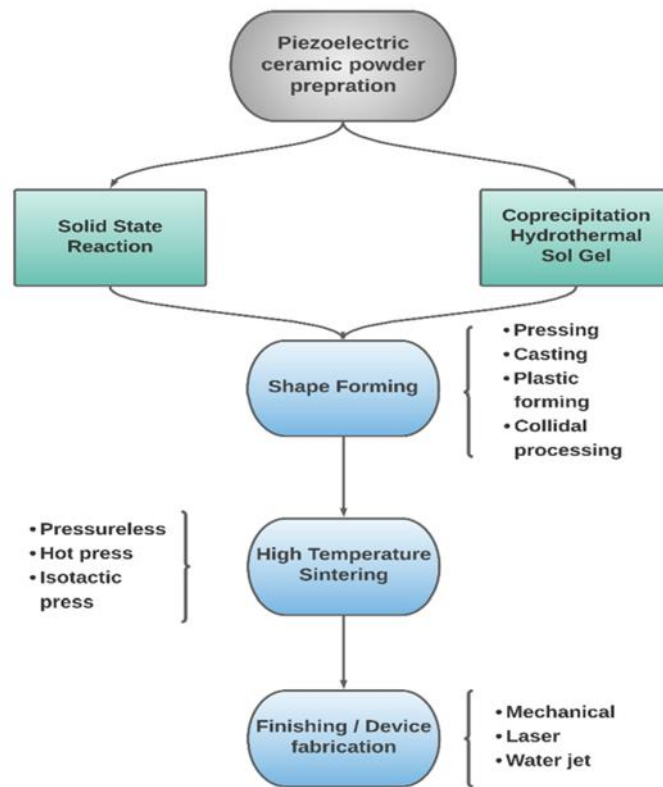
Figure 23 Schematic of powder processing for advanced ceramics

3.3.1 Solid-State Reaction:

One of the most prevalent ways for producing ceramic materials for piezoelectric applications is the solid-state process. Precursors such as hydroxides, metal oxides, and salts are combined and reacted in solid form in this process. The traditional method of preparing multicomponent ceramics necessitates continual operations of mixing, solid-state reaction, and regrinding. Multicomponent phases are formed because of solid-state processes. The reactions might result in the agglomeration or development of powder clusters that require additional grinding to lower the particle size to micrometer level. Milling beyond the sub-micron level can be challenging with hard materials. [42, 43]

Advantages:

1. Because of their low cost, high yield, and simplicity, they were frequently employed to make PZT powders.
2. With the advancement of high-energy milling technology, particle size less than the micron level can be achieved with acceptable chemical homogeneity, and narrow size distribution can be easily manufactured in PZT.

Disadvantages:

1. There is a wide size variation and inadequate purity and homogeneity of the powder in hard materials.
2. Calcinating the mixture at high temperatures enhances the agglomeration loss of volatile oxides, such as lead oxide in PZT, and the production cost.

3.3.2 Coprecipitation:

Coprecipitation is a popular ceramic powder synthesis process for producing mixed oxides from solution. It begins by creating a supersaturated solution with the precipitating ingredient. The precipitated powder is then filtered from the solution and dried. The powder is then thermally decomposed to produce the desired ceramic. Several factors of the coprecipitation process may be regulated, including temperature, pH level, precursor concentration, and mixing speeds [44, 45].

Advantages:

1. The produced products are of high purity, content, and morphology.
2. Fine particle size with high purity and a narrow size distribution may be created by adjusting the reaction conditions.
3. Producing a high-quality product is relatively affordable.

Disadvantages:

1. Differences in the rate of precipitation of specific chemicals can generate microscopic inhomogeneity.
2. Calcination, like other synthesis processes, can produce agglomerates in general.

3.3.3 Hydrothermal Synthesis:

Hydrothermal synthesis is a wet chemical synthesis process that produces anhydrous, crystalline ceramic powders in aqueous environments. The solution or suspension of components in an aqueous media is treated at extreme temperatures and in pressurized containers known as vessels in this procedure. High temperatures typically range from the boiling point of water to the critical temperature of 370°C. The pressure can rise to 15 MPa at the same time. The unique

circumstances of extreme pressure and temperature confine a solution phase. This causes fast phase change kinetics in the medium, which is facilitated by mass transport [45].

Advantages:

1. Greater control over reaction kinetics due to temperature and pressure.
2. The final products are of high purity, content, and shape.

Disadvantages:

1. Maintaining high temperature and pressure conditions is rather costly.
2. Because of the operational circumstances, there is a high risk of accidents and safety difficulties.

3.3.4 Sol-Gel:

This method entails creating an amorphous gel from the solution, which is subsequently dehydrated at low temperatures. Metal oxides and salts undergo hydrolysis in a gelation agent, resulting in cross-linking and branching. The polymerization procedure produces a dense three-dimensional structure that retains mixing and results in regulated composition at the molecular level, preventing any segregation. Because the early precursors are soluble, the composition is retained at the molecular level during the gelation process. The gel with a three-dimensional matrix is then dried by heating at a low temperature. The temperature is often lower than in any other method of synthesis. [46, 47]

Advantages:

1. This method may yield exceedingly pure ceramics with exceptional uniformity.
2. Considerable structural control over the resultant powders via parameter management.

Disadvantages:

1. It is a time-consuming procedure with complex circumstances and parameters.

2. The method is extremely costly due to the usage of specialized raw materials and the calcination of the amorphous powder at elevated temperatures to create the necessary crystalline structure.
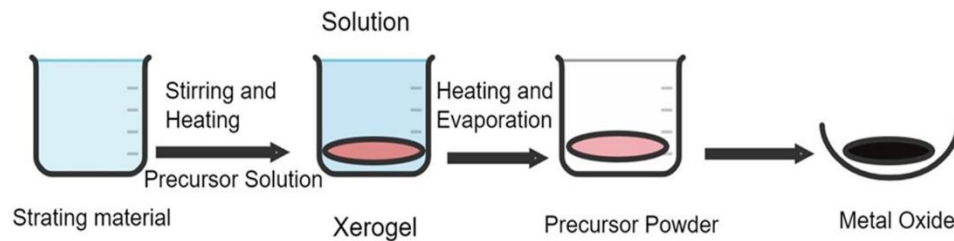
Figure 24 Schematic of the sol-gel process

3.4 Powder Processing Techniques:

3.4.1 Dry Powder Pressing:

The typical method for producing compressed powders is dry powder pressing. This process works by exerting pressure and compacting the dry powder that has been put inside the die. This manufacturing method can produce complicated forms at a rapid pace. Powder is compacted by placing it in a stainless-steel die and applying severe pressure in the compaction direction using a hydraulic press.

Figure 25 Die used for powder pressing.

3.4.2 Tape Casting:

It is a shape-forming process used to cast complicated forms and geometrical elements. Slip casting, which is commonly utilized for traditional ceramics, may also be used for advanced ceramics. The primary step in the process is the slip, which is a suspension of polar molecules in a fluid containing suspended ceramic particles. The slip is then poured into the porous mould. Capillary action sucks liquids out of the mould, creating a solid layer of ceramic on the mould

surface. The mould is typically composed of plaster of Paris, and the suspension is created in water. This technology, which is a reasonably inexpensive, can produce water. This technology, which is reasonably inexpensive, can produce complicated thin-walled structures with uniform thickness[3].
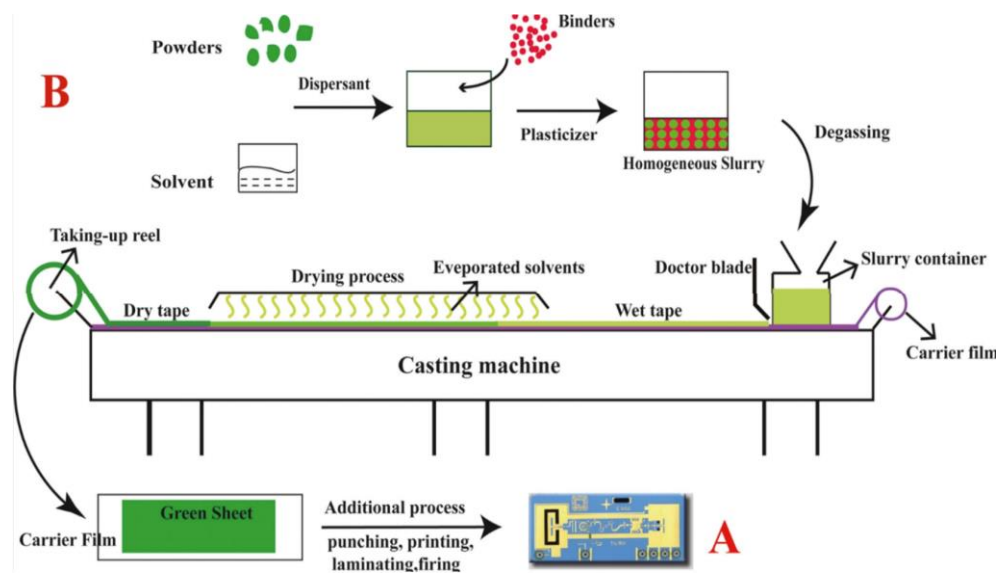
Figure 26 Process of tape casting [3].

3.5 Synthesis of PZT ceramic:

The piezoelectric ceramic was created using the more typical solid-state approach, which involves the use of reagent grade oxides. To produce lead-Oxide (yellow hue), lead (Pb) is calcined at 700°C. Later, lead-Oxide was combined with other local oxide precursors such as titanium dioxide (TiO_2; 99.9%) and ZrO_2 with the nominal composition Pb (Zr0.52 Ti0.48) O3. For 8 hours, the oxides mixture was milled using Ethanol and Zirconia balls as milling media. The slurry was dried in a box oven at 90°C for 12 hours before being crushed into yellow pellets with a diameter of 1mm and a thickness of 11.6 mm using a hardened stainless-steel die under 3t pressure. As a binder, 5% PVA aqueous solution was added to the mixed powder. The pellets were sintered in an air-cooled box furnace at temperatures ranging from 1000°C to 1200°C for 4 hours at intervals of 550°C for a constant period of 30 minutes, with heating and cooling rates of 5°C/min.

Figure 27 Graphical schematic for synthesis of PZT

Chapter 4:

Experimentation

Characterization gives information about the material structure, chemical composition, and material qualities linked to the application. To learn more about the morphology, structure, composition, and electromechanical characteristics of the piezoceramic material, the properties of synthesised PZT ceramic are examined using a variety of characterisation techniques. In this chapter, these strategies are briefly covered.

4.1 XRD (X-ray diffraction):

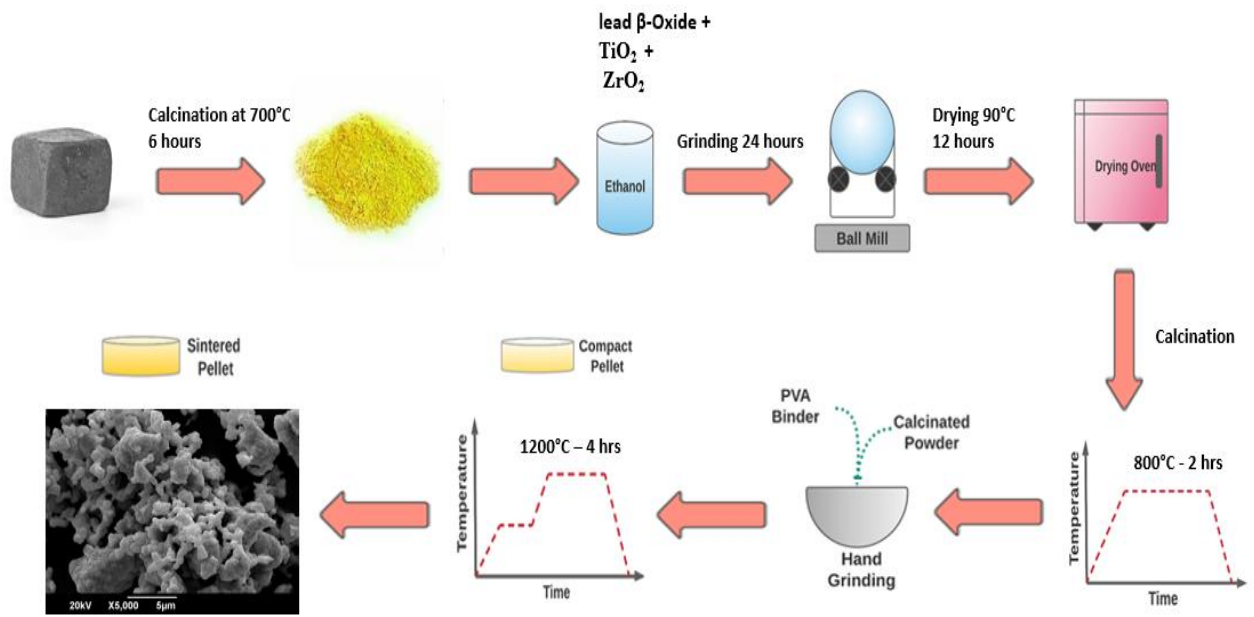The use of XRD is a method for determining the degree of crystallinity, crystal structure, stresses, crystal defects, lattice constant, and geometric confirmation of hidden structure. The powder diffraction method, the Laue method, and the rotating crystal method are three techniques that can be used to determine the crystal structure. The two main processes are utilised in the powder diffraction approach. These procedures are

1. Debye Sherrer method.
2. Diffractometer method.

The specimen of substance was a finely ground powder. Copper, molybdenum, and other metals can be employed as targets. For analysis, an XRD was used with a Cu (k-alpha) 1.54060 source.

4.1.1 Basic Principles of XRD:

XRD is used to gather a variety of data points based on the dual nature of wave and particle nature. In X-ray diffractogram analysis (XRD), a beam of X-rays with a specific wavelength is directed at a powder sample and reflected by a crystal structure. The interference only occurs when the incident angle and the reflected angle are exactly equal. The diffraction of X-rays by crystals is demonstrated by Bragg's Law.

$$n\,\lambda = 2d\,\mathrm{Sin}\theta \dots\dots\dots\dots\dots\dots(\textbf{4.1})$$

Where,

d is a separation between microscopy planes.

λ is X-ray wavelength.

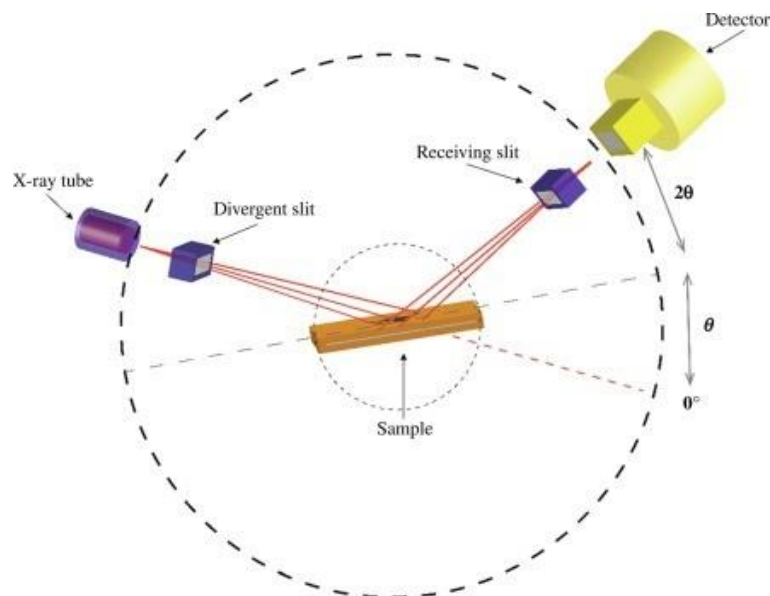$\mathrm{Sin}\theta$ is the angle between the incident beam and reflected beam.

Figure 28 Working principle of XRD.

According to Bragg's law, the path difference between the planes must equal 2d Sin θ for the incident ray to be reflected. The glancing angle and wavelength have an inverse connection in which the wavelength drops as the angle rises and vice versa [3]. The principle outlined above is that reflection occurs when the angle of incidence (θ) is greater than or equal to twice the distance between the crystal planes (2d). A schematic and working principle of this concept is depicted in Figure 28.

The sample must first be ground into a fine powder to carry out this experiment. The powder is then positioned on a glass or aluminum rectangular plate. The powder sample is subsequently exposed to a monochromatic X-ray beam.

4.1.2 Lattice Constant:

The lattice constant, commonly known as the lattice parameter, defines the unit cell of a crystal. The length of one edge or the angle produced between two edges of the unit cell can both be used to describe this property. The following equation is used to calculate the distance between the lattice points and yields the lattice constant:

$$\boldsymbol{\alpha} = \frac{\lambda\,(h2+k2+I2)}{2\sin\theta} \quad \text{..................................} \quad (4.2)$$

The above equation shows that lattice constant is (**α**) the wavelength of X-ray incident is 1.54Å for Cuk (**α**), miller indices.

4.1.3 Crystallite Size:

The experiment's diffraction pattern is compared to JCPDS cards to recognize and validate it.

The particle size of a material can have a significant impact on its structural characteristics, and XRD can precisely measure the homogenous and inhomogeneous peaks of nanomaterials. As the angle is increased in inhomogeneous materials, a wide range of diffraction peaks are produced because the strains can differ from crystal to crystal, even within a single crystal. From the peak width of the diffraction pattern, the crystallite size (D) can be calculated using Scherer's formula [48].

$$\mathbf{D} = \frac{K\lambda}{B\,Cos\theta} \cdots\cdots\cdots\cdots\cdots\cdots (4.3)$$

Where,

B in the above equation denotes full width half maximum.

θ is the angle called diffraction angle.

K is known as Scherer's constant depending upon crystal size.

4.1.4 X-Ray density

If the lattice constant for each sample is known, the material density can be determined using XRD and then calculated using the formula.

$$\rho_{\mathbf{x}} = \frac{8M}{Na3} \cdots\cdots\cdots\cdots\cdots\cdots\cdots\cdots (4.4)$$

4.1.5 Measured Density:

We may learn about the inherent qualities of materials from their measured density, also known as bulk density. The standard calculation formula

$$\rho_{\mathbf{m}} = \frac{m}{r2h} \cdots\cdots\cdots\cdots\cdots\cdots (4.5)$$

'm' represents mass, 'r' represents the radius, 'h' represents the thickness of the pressed pallet.

4.1.6 Porosity Density:

Porosity density is a measure of the strength of a pellet and its porousness, or the property of being porous. Increasing the concentration of doping material in the sample can result in an increase in the porosity fraction. This can be calculated using the formula:

$$\mathbf{Porosity\ fraction} = 1 - \frac{\rho m}{\rho x} \cdots\cdots\cdots\cdots\cdots\cdots\cdots (4.6)$$

4.2 SEM (Scanning Electron Microscopy):

For morphological analyses of materials, scanning electron microscopy (SEM) is a vital tool. By concentrating an electron beam onto the sample, it creates a picture. Greater depth of field and better resolution are just two benefits of SEM over conventional microscopy. Instead of using lenses and visible light, it uses electron beams and electromagnets, which offers a far greater level of resolution. The material and the electron beam's interface results in fine-grained surface characterisation imaging. The electron beam in a conventional SEM can be used to achieve a focussed spot of 5 nm. SEM generates various forms of imaging, such as: [48]

1. Secondary electron images.
2. Back-scattered electron image.
3. Elemental X-ray map.

A highly energised electron might collide with an atom in an elastic or inelastic manner. When an electron collides with an atomic electron, it does so in an elastic manner, but when it collides with an atomic nucleus, it does so in an inelastic manner. In elastic collisions, some of the energy may be transferred to the nucleus, which may cause the emission of a secondary electron with an
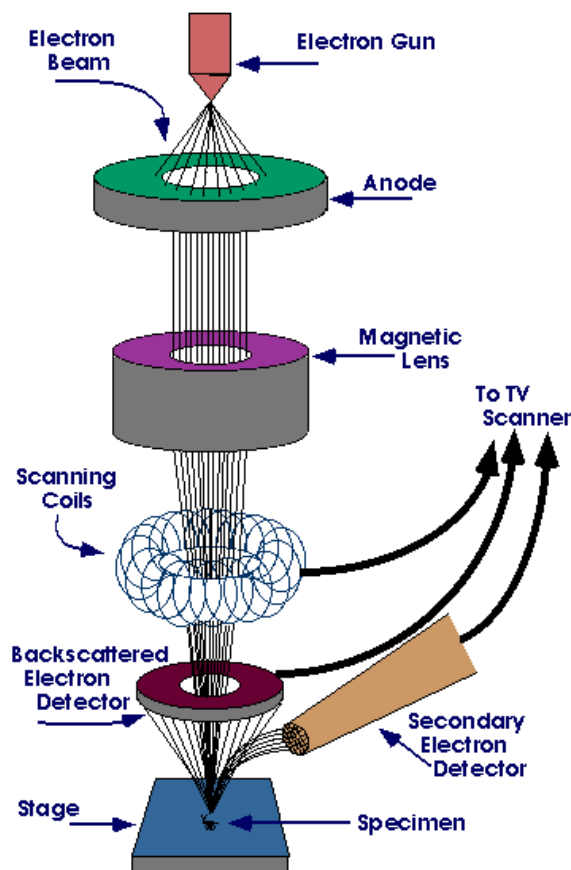

Figure 29 Working mechanism of SEM apparatus.

energy of under 50 eV. High-energy electrons that have the same energy as the incident primary electron are backscattered electrons. Backscattered electrons are produced in a scanning electron microscope (SEM) when high-energy electrons are scattered back towards the detector; these electrons reveal the composition and topography of the material. Additionally, primary electrons can excite the sample's atoms, causing them to release X-ray photons when they return to their ground state. These X-rays can also be seen with a scanning electron microscope (SEM), and they reveal the elemental makeup of the sample.

The resolution of the instrument is defined as,

$$R = \frac{\lambda}{2NA} \dots\dots\dots\dots\dots\dots (4.7)$$

Where,

Wavelength of the electron is represented by λ.

NA is known as a numerical aperture.

SEM can reveal the chemical composition and distribution within the sample in addition to structural details about bulk and nanostructured materials. Utilizing methods like energy-dispersive X-ray spectroscopy (EDS), which can locate and map the distribution of elements within the sample, this is accomplished. SEM may also produce topographical images and three-dimensional images, both of which are helpful for comprehending the sample's shape and surface characteristics. When combined with other research methods, electron microscopy-based analysis can help in the thorough characterization of materials by revealing important details about their physical, chemical, and mechanical properties [49].

4.3 FTIR (Fourier Transform Infrared Spectrometry):

An effective method for examining materials with functional groups is infrared spectroscopy. The relationship between matter and the electromagnetic field is investigated in the infrared spectrum. This is accomplished by examining how well the sample absorbs infrared light. The vibrations of the sample's constituent molecules are energised when it absorbs infrared light, and this resulting spectrum can reveal details about the sample's chemical composition and structure. The frequency of the electromagnetic field and the motions of the molecules affect how much radiation the sample can absorb. Numerous compounds, including polymers, organic molecules, and minerals, can be identified and characterised using infrared spectroscopy, which is frequently used in the fields of chemistry, biology, and materials science. An in-depth understanding of a material's chemical composition and physical structure can be obtained using the robust and adaptable technique of infrared spectroscopy. A popular technique of infrared

spectroscopy known as Fourier Transform Infrared (FTIR) spectroscopy analyses the amount of infrared light absorbed by a sample at wavelengths. Understanding the frequencies at which various compounds absorb infrared light is crucial to interpret FTIR spectra. The Fourier transform, which mathematically connects a sample's time-domain signal to its frequency-domain spectrum, underlies the operation of the FTIR spectrometer. A Fourier transform pair, which transforms the time-domain signal into a frequency-domain signal and vice versa, is used to mathematically explain this.

$$\mathbf{F}(\boldsymbol{\omega}) = \int_{-\infty}^{+\infty} f(x) e^{imx} \, \mathbf{dx} \quad \dots\dots\dots\dots\dots\dots\dots(4.\,8)$$

And the conflicting form of this equation is

$$\mathbf{F}(\boldsymbol{\omega}) = \frac{1}{2\pi} \int_{-\infty}^{+\infty} f(x) e^{imx} \, \mathbf{dx} \quad \dots\dots\dots\dots\dots (4.\,9)$$

Where,

ω is the regularity.

X is ophthalmic path variance.

(ω) is the spectrum.

$f(x)$ is the interferogram [50].

A heated black-body source emits infrared radiation, and an aperture regulates the quantity of radiation. The radiation is then directed into an interferometer for spectral encoding. The sample receives the beam and can either transmit or reflect the light. The detectors, which are intended to measure the interferogram signals, do the final measurement. The infrared spectrum is produced using a mathematically complex Fourier Transform once the observed signals are transmitted to a computing platform.
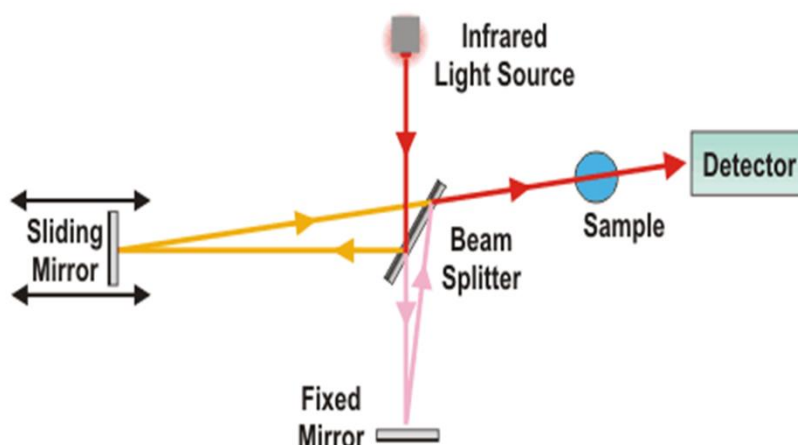

Figure 30 Working principle of FTIR spectroscopy.

This procedure entails transforming the interferogram's time-domain signal into a frequency-domain signal that symbolizes the sample's absorption spectrum. FTIR spectroscopy is a highly

sensitive method that can identify even minute changes in chemical composition and structure, making it ideal for the scientific field. [50, 51]

Fourier Transform Infrared Spectroscopy is referred to as FTIR. It is a kind of spectroscopy that examines how matter and electromagnetic radiation interact in the infrared spectrum. In FTIR, a certain collimated, monochromatic light source generates an interferogram at the detector that resembles a sinusoidal wave. The optical difference between the two legs of the interferometer changes by precisely one specific wavelength of the inbound radiation when the light intensity changes from one maximum interferogram to the next maximum. There are three main types of FTIR.

1.   Transmission FTIR spectroscopy.
2.   Emission FTIR spectroscopy.
3.   Reflectance FTIR spectroscopy.

Since the amount of infrared radiation absorbed by the sample can change even slightly, FTIR detectors are extremely sensitive and can pick up on these changes. Comparatively to other kinds of spectrometers, FTIR uses a single moving mirror, which lowers the likelihood of mechanical failure. FTIR is a trustworthy tool for study and analysis since its readings are extremely exact and repeatable. The adaptability and flexibility of FTIR have also enabled the creation of new sample methodologies. [50]

4.3.1 Sample Preparation for FTIR:

In order to analyse solid materials using FTIR spectroscopy, this process of making KBr pellets is frequently utilised. An appropriate diluent for the sample is KBr, an alkali salt that does not absorb in the IR range. The sample is uniformly dispersed in the KBr matrix by mixing it with KBr in a precise ratio and pressing it into a pellet, enabling the acquisition of a representative IR spectrum. A consistent and reproducible pellet can be produced by paying attention to the size and pressure of the pellet die.

4.4 Dielectric and Electromechanical Properties:

4.4.1 Dielectric Properties:

Dielectric properties of materials, including dielectric loss, dielectric constant, tangent loss, and electric modulus, can be determined using an LCR meter bridge. The capacitance of pellets finds out by using an LCR meter, and for dielectric constant calculation following formula is used.

$$\varepsilon' = \frac{C*d}{\varepsilon 0 A} \cdots\cdots\cdots\cdots\cdots\cdots\cdots\cdots\cdots (4.10)$$

A represents the cross-sectional area of the pellet, C represents the capacitance, d represents the thickness, and ε0 is the permittivity constant of free space and its value $8.85418782 \times 10^{-12}$ F/m. The imaginary part that corresponds to energy dissipation losses is calculated by using the following relation.

$$s'' = \varepsilon' + D \ldots\ldots\ldots\ldots\ldots\ldots (4.11)$$

Dielectric materials experience some power losses as a result of friction, damping, and charge dissipation. The tangent loss factor and D-factor are expressed mathematically.

$$\mathbf{Tan\delta = D =} \frac{s}{\varepsilon'}^{FF\cdots\cdots\cdots\cdots\cdots\cdots} (4.12)$$

AC conductivity of material at room temperature can be calculated by using.

$$\sigma_{ac} = \omega \ \varepsilon_0 \ \varepsilon'' \ldots\ldots\ldots\ldots\ldots\ldots (4.13)$$

4.4.2 AC Impedance:

Using an AC impedance test, the pellets' dielectric qualities were examined at room temperature. The measurement comprised determining the resistance (R) and reactance (X) over a frequency range of 100 Hz to 5 MHz The complex variable known as impedance, which has both a real and an imaginary component, was also measured. The imaginary portion stands in for the reactive component, whereas the actual portion is resistance. The real and imaginary components of impedance can be used to represent the relationship between resistance and reactance in a circuit.

$$\mathbf{Z = R + jX} \ldots\ldots\ldots\ldots\ldots\ldots\ldots (4.14)$$
$$\mathbf{Z' = R = |Z| \ cos\theta} \ldots\ldots\ldots\ldots\ldots\ldots (4.15)$$
$$\mathbf{Z'' = X = |Z| \ sin\theta} \ldots\ldots\ldots\ldots\ldots\ldots (4.16)$$

4.5 RAMAN:

A powerful technique for characterization and identifying different kinds of materials, including solids, liquids, and gases, is Raman spectroscopy. It is a technique that offers knowledge about the molecular vibrational modes of a material without causing damage, invasiveness, or touch. The inelastic scattering of light by a sample is the foundation of the Raman method. A molecule may be excited to a higher vibrational state when a photon of light interacts with it. The Raman shift is the process by which the molecule relaxes back to its ground state by releasing a photon of light with a different energy.

When a molecule scatters light, the oscillating electromagnetic field of the photon causes the molecular electron cloud to become polarised, which elevates the molecule's energy and transfers the photon's energy to it. This is the development of a very short-lived complex between the photon and the molecule, which is generally referred to as the virtual state of the molecule. Since the virtual state is unstable, the photon is quickly reemitted as scattered light.

A spectrometer is used to collect and analyse the scattered light in the Raman technique, which includes shining a laser beam of a certain wavelength on the sample. Surface-enhanced Raman scattering (SERS) and resonance Raman scattering (RRS) are two techniques that can be used to improve the signal of the generally weak Raman scattered light.
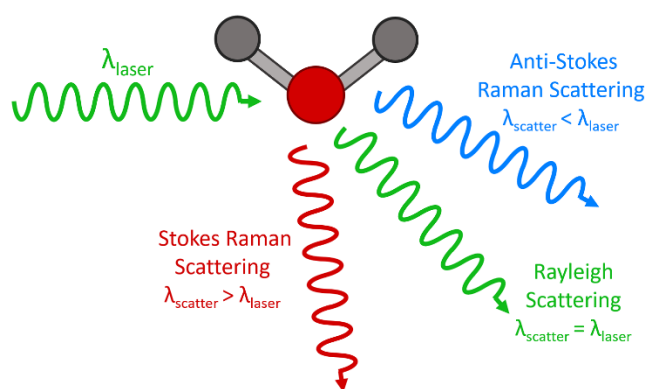

Figure 31 Three types of scattering processes that can occur when light interacts with a molecule.

4.6 Thermogravimetric Analysis (TGA):

When materials are heated under controlled conditions, the weight loss and thermal stability of the materials are assessed using a thermal analysis technique called thermogravimetric analysis (TGA). The analysis entails determining a sample's weight as a function of temperature or time while it experiences a predetermined temperature ramp. The composition, thermal stability, and degrading behaviour of materials can all be learned via the TGA.

In TGA, the sample is heated in a controlled environment, often air or nitrogen, while it is contained in a crucible. The sample's temperature is raised gradually and steadily, and its weight is continually measured as a function of temperature or time. The rate of weight loss determines the material's thermal stability, and the temperature at which there is a noticeable weight loss identifies thermal disintegration or degradation.

For dynamic TGA, a graph displaying mass as a function of temperature is frequently used to display data from thermogravimetric analysis. A plot of the sample weight loss (or gain) as a

function of temperature or time often constitutes a TGA thermogram. Most of the time, the first weight loss is related to the loss of moisture or other volatile substances in the sample. The subsequent phase of weight loss is frequently correlated with the breakdown of the sample's organic or inorganic constituents. The breakdown temperature and rate can reveal details about
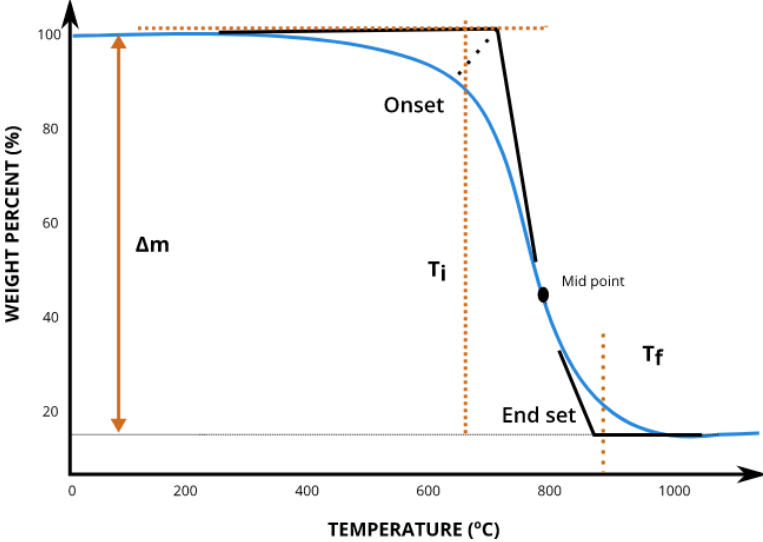

Figure 32 Thermogram of TGA

the material's composition and thermal stability.

Chapter 5

Results and Discussion

5.1 Lead Oxide (β-PbO) Results:

5.1.1 XRD

For synthesis of PZT, lead was extracted from lead acid batteries. Lead was further calcined for the synthesis of β-PbO (yellow colour). As PbO is one of the major components for synthesis of Lead zirconate titanate, its properties were also studied. As shown in figure 33 the peak (1 1 1), which was the strongest peak according to the JCPDS card sheet, was plainly visible as having the highest intensity representing β-PbO (orthorhombic). There were no other peaks that might have been impurity or intermediate peaks, like lead (II) oxide hydrates (3PbO.H_2O), to be found. In the β -PbO unit cell, two oxygen sublayers are sandwiched between two lead sublayers. This arrangement created calliope (staggered) Pb-O chains, with the lead displaying asymmetric square pyramidal coordination. The peak at (020) is attributed to monoclinic phase Pb_2O_3 JCPDS card number: 00-023-0331. The natural mineral form of lead (II) oxide known as massicot has an orthogonal lattice structure with lattice parameters of a = 5.492159 Å, b = 5.893166 Å, and c = 4.755345 Å.
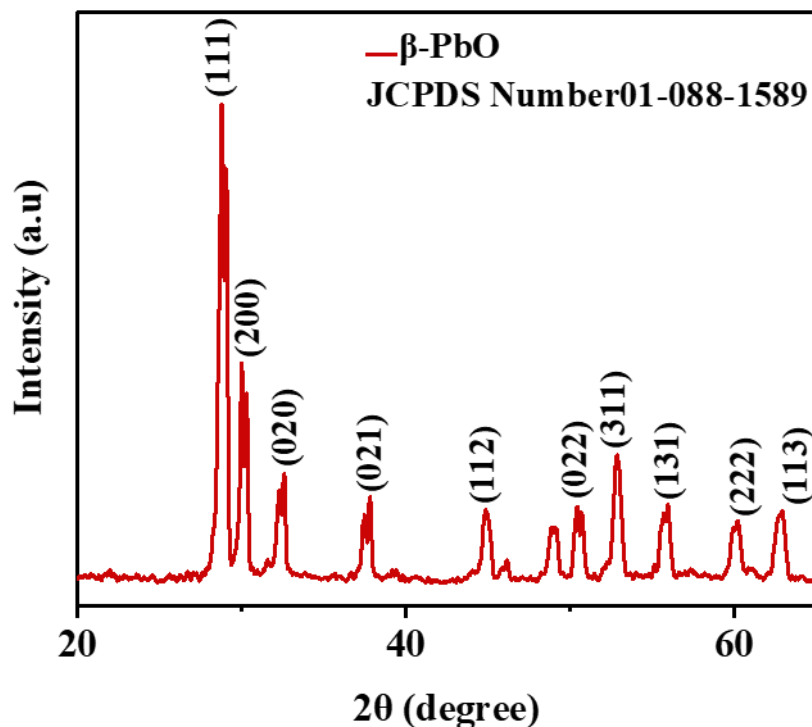

Figure 33 XRD pattern acquired from as-synthesized β-PbO powders.

5.1.2 Morphological analysis:

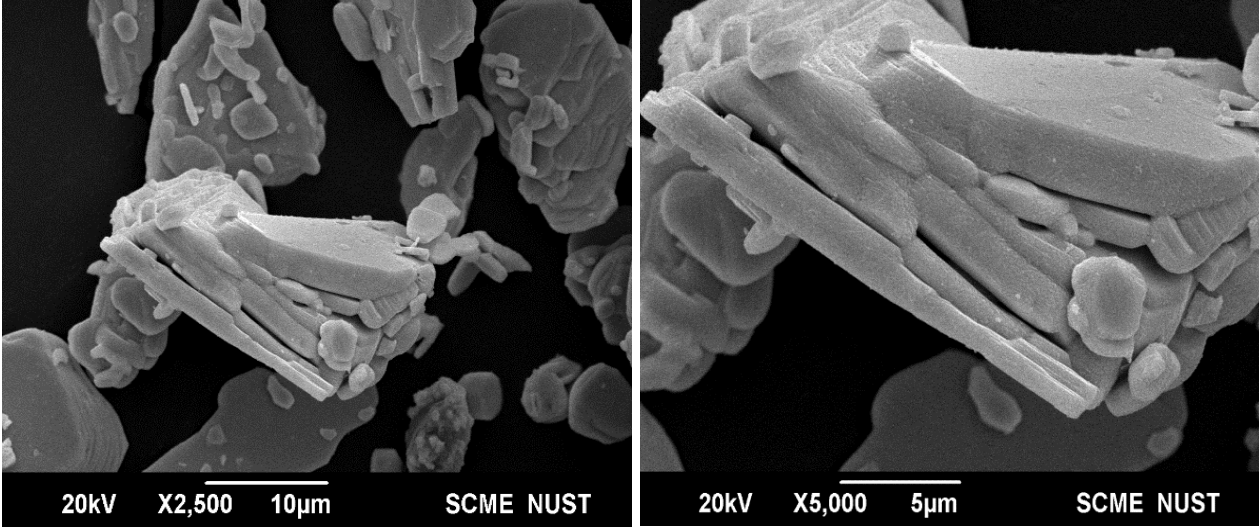SEM demonstrated that precipitate has a flake-like structure in layered form with an average size
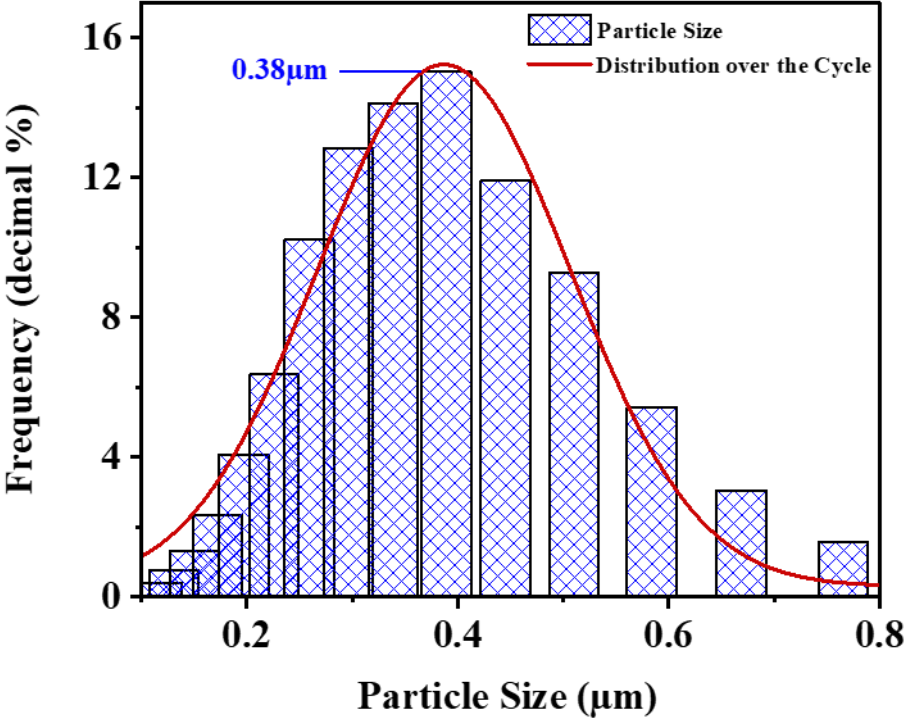

Figure 34 SEM images of lead Oxide

Figure 35 Particle Size of β-PbO powders.

of 0.38µm found via using particle size analyzer, as can be seen Figure 35. The particles were considerably smaller than the initial lead paste. As a result, the precipitate's specific surface was greater. region, which will give the creation of piezoelectric material a good response surface area Figure 36.

5.1.3 FTIR:

By using FTIR, the chemical bonding of lead oxide powder was investigated. On the FTIR spectra, two extremely strong peaks at 466.74 cm^{-1} and 557.39 cm^{-1} signify the presence of lead and oxide [52].
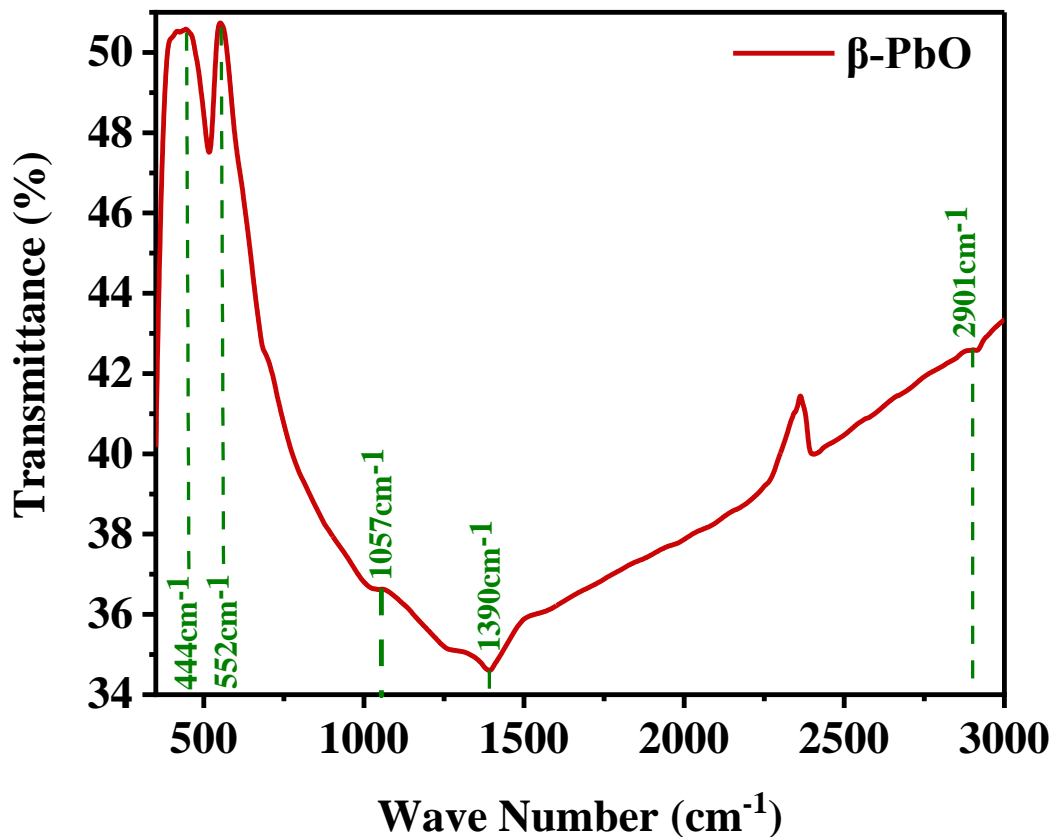

Figure 36 FTIR pattern acquired from β-PbO powder.

The emergence of the transmission peak at 444cm^{-1} denotes the presence of the (PbO) stretching vibration mode, whereas the transmission peaks at 1057.03 cm^{-1} is connected to the (C=O) stretching vibration modes and denote a minimal contribution of CO_2 dissolution from air containment, respectively. It is known that a second peak at 1390 cm^{-1} represents the stretching vibration of the carboxyl group (C-O) Figure 36.
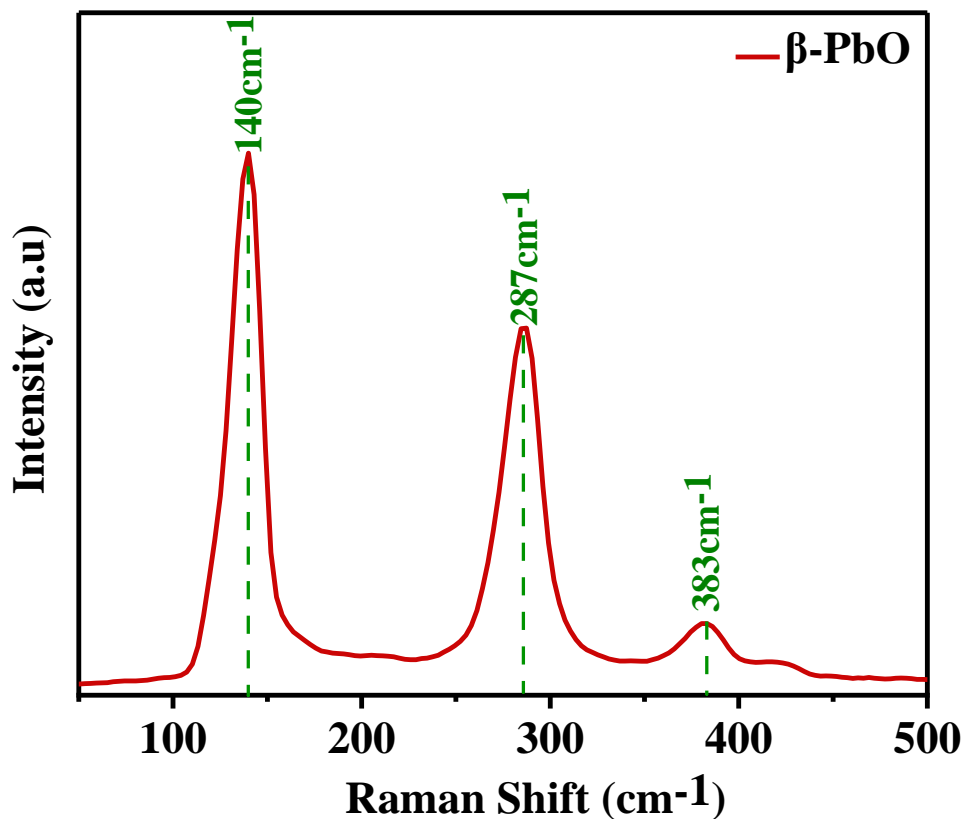
5.1.4 RAMAN:

Figure 37 RAMAN Spectrum of β-PbO powder.

Since ancient times, massicot has been utilized as a yellow pigment. It is an excellent Raman scatterer and seems stable in the experimental setting. Band at $140cm^{-1}$ clearly corresponds to the massicot Figure 37. The acquired spectra are consistent with other spectra those of massicot published in the literature [53].

5.1.5 TGA and DSC:

Thermal gravimetric analysis (TGA) and differential scanning calorimetry (DSC) were performed to a temperature of 700 °C with ramp rate of 10°C/min to assess the thermal stability of the PbO, as shown in Fig 38. PbO powder that has been manufactured is extremely stable up to 50°C. After 50°C, the powder begins to decompose, reaching its maximum breakdown at roughly 290° with a weight loss of 0.3% that may be explained by the conversion of lead dioxide to lead oxide. This happens because during the thermal decomposition process, the oxidation number of the lead ions remains constant. The endothermic peak shows the phase change happening due to conversion of PO_2 to PbO.
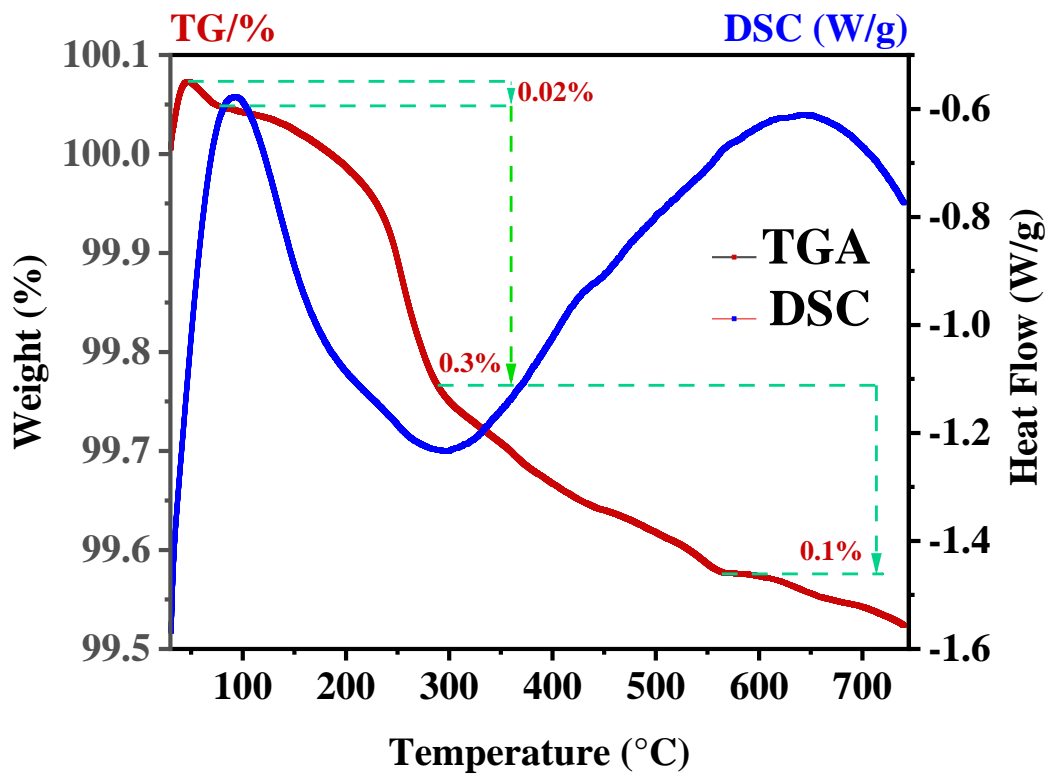
Figure 38 TGA/DSC of β-PbO

5.1 PZT Results:

5.2.1 XRD:

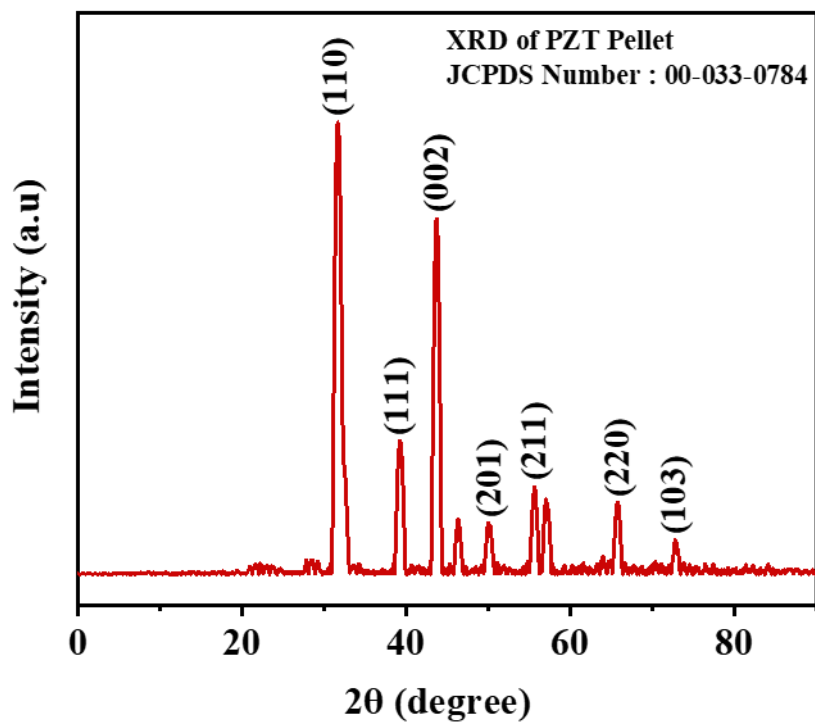

Figure 39 XRD pattern of PZT Pellet

XRD patterns of PZT were analyzed between 2θ 20°-80° for the time spam of 45 minutes. Later these results were put for further analysis using PANalytical-X'pert high score program. The diffraction peaks of β-PbO and are indexed according to the standard JCPDs card (No. 01-088-1589) and (No.00-033-0784) along with the hkl values. It is established through the analysis that the acquired results are consistent with past studies and that the structure of PZT is a perovskite structure. It is also evident from the patterns that the greatest powerful reflection (110) occurs at 231.14°, which is quite close to the value given in the literature for pure PZT ceramic phase [54] [55]. Figure 39 XRD displays the (111) pattern for the tetragonal phase together with (002) and (201) reflections. In all the XRD patterns, only the peaks of the PZT perovskite phase could be seen except after (201) which correspond to the electrode applied to the pellet.

5.2.2 Morphological analysis:

Microstructure analysis was done using SEM. Prior research suggested that the commercial PZT powder is composed of spherical particles with diameters between 10 and 50 µm. All large particles were crushed after milling the powders for 10 hours with ethanol as milling media. Calcination at 820°C for 2 hours with ramp rate of 10°C/min gave the perovskite structure. It was observed that the final PZT powder had a larger particle size dispersion due to an increase in heating rate and the presence of large particles. This fits in with additional findings [2]. The product is agglomerated by ultrafine particles with the size of approximately in the distribution range of 2.5 –14 µm shown in figure 41. As shown in figure 42 the powder was refined to contain grains that were of average 6.4µm in size. The micrographs reveal relatively dense and uniform microstructure.

To determine chemical compositions following calcination, energy-dispersive spectroscopy (EDS) was used. The PZT- EDS spectrum is depicted in Figure 42, PZT is confirmed to contain lead (Pb), zirconium (Zr), titanium (Ti), and oxygen (O).
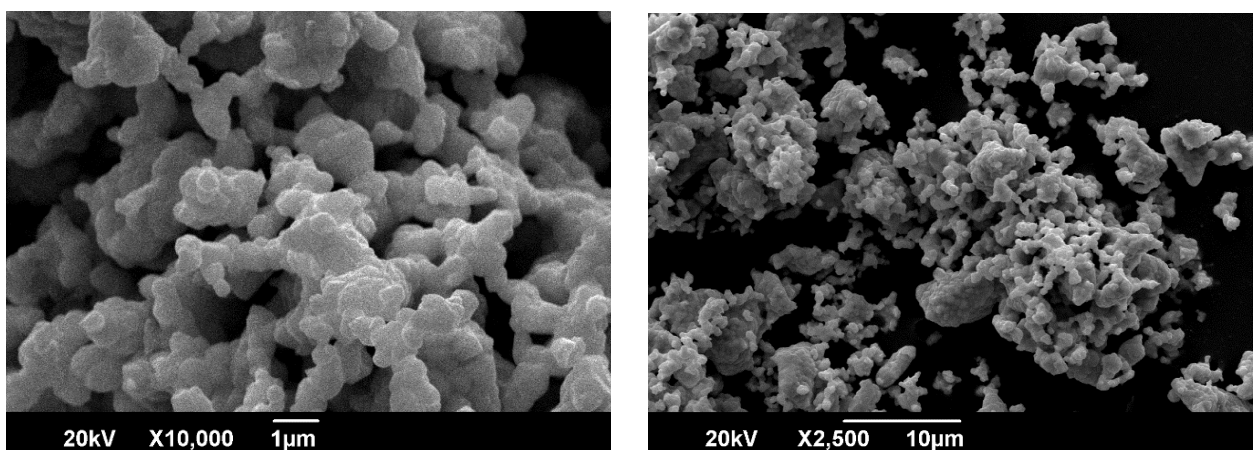

Figure 40 SEM images of pure PZT Ceramic
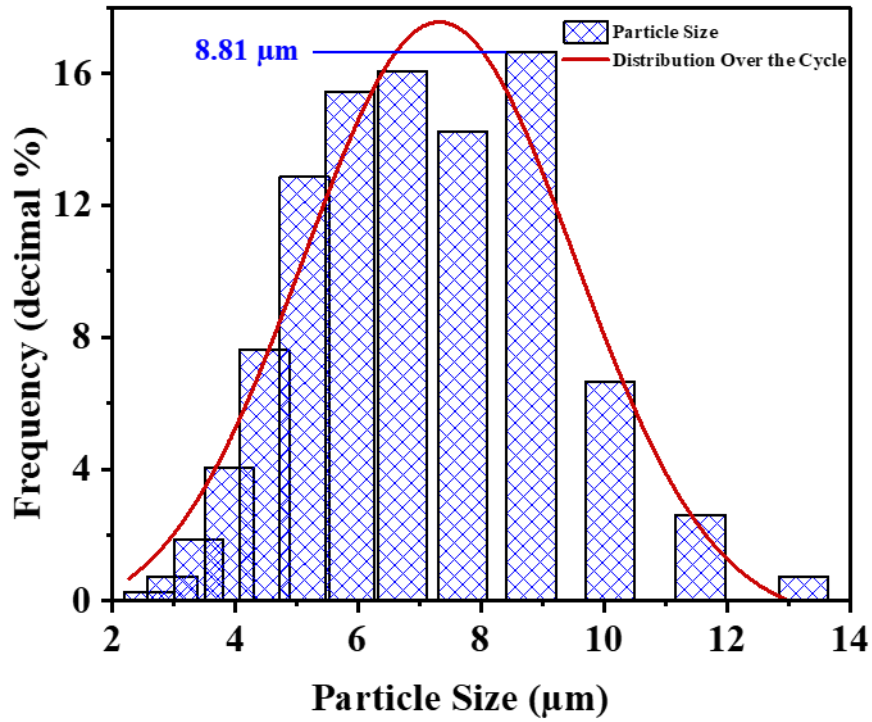
Figure 41 Particle Size Distribution of PZT
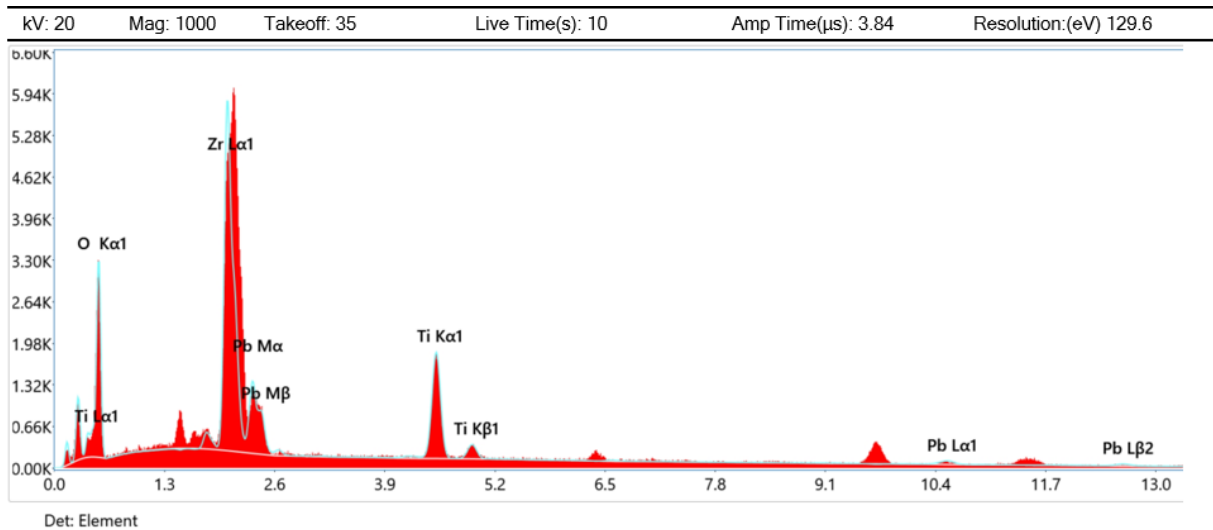
Figure 42 Elemental composition of PZT by EDS

5.2.3 FTIR:

The core ions zirconium (Zr^{4+}) and titanium (Ti^{4+}) occupy the B-sites in PZT, which is a form of perovskite (ABO_3 type) in which the A-sites are filled by lead (Pb^{2+}) ions. With six coordinating oxygen atoms, these center ions form an octahedron. Dependent on the Zr/Ti ratio, this can exist in a variety of phases, and once it reaches a temperature above Curie, it develops a cubic structure. According to the Zr/Ti ratio, the cubic distorts below Curie temperature to create either

tetragonal or rhombohedral structures. The MPB, which demonstrates the presence of both tetragonal and rhombohedral phases, separates these two phases. However, other studies indicated the creation of a new monoclinic phase around the MPB. E and A_1 symmetry elements emerge from the cubic phase's transformation into the tetragonal phase of the C_{4v} point group, and A´ and A´´ symmetry elements emerge from the tetragonal phase's transition into the monoclinic phase. The typical IR active broad band of PZT rhombohedral phase is seen at around 580 cm^{-1} at room temperature, shifting up to about 690 cm^{-1} in tetragonal phase [56]. Using a Fourier transform infrared (FTIR) spectroscope, molecules in the solid phase were examined between 400 cm^{-1} and 35000 cm^{-1}. The FTIR spectra after being calcined at 820° C is
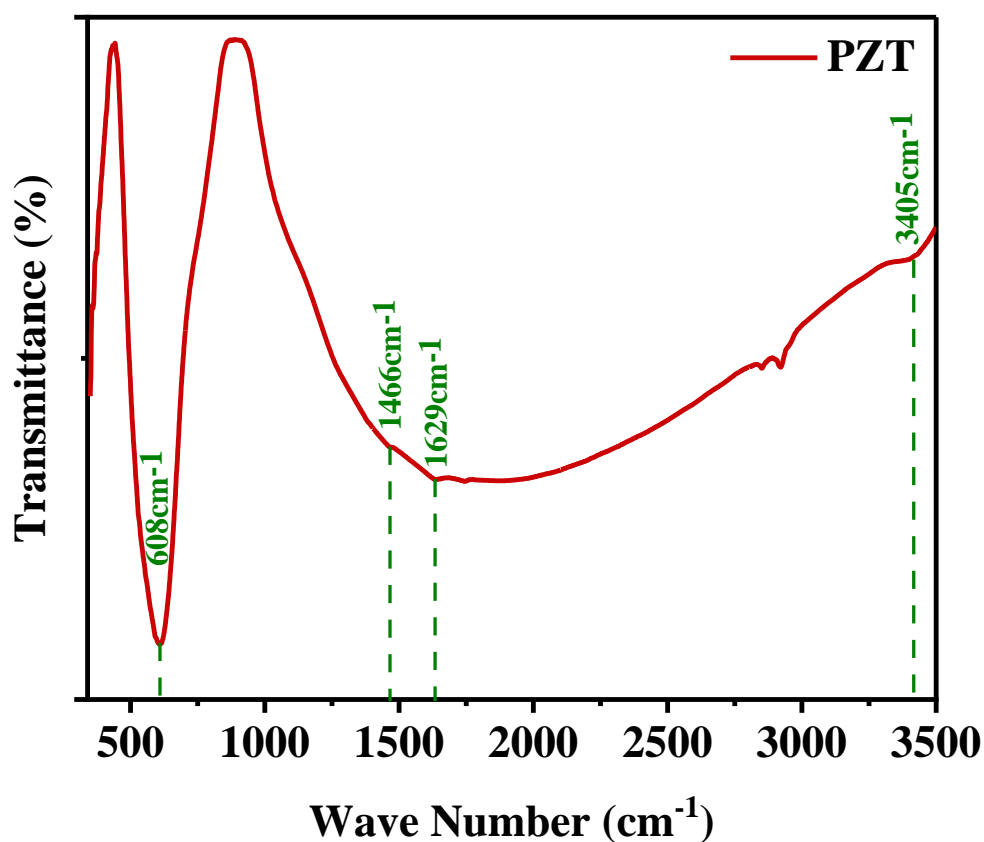

Figure 43 FTIR spectra after calcination PZT at 820°C

depicted in Figure 43. The O-H groups' stretching vibration caused by their hydrogen bonding to vibrate at a broad absorption band of 3435 cm⁻¹. Peaks at the 1637 cm⁻¹ and 1400 cm⁻¹ bands correspond to the symmetric and asymmetric C-O vibration of -COO groups, respectively. The peak at ∼608cm⁻¹ is present which is attributed to BO_6 octahedral vibrations. This confirmed the formation of tetragonal phase of PZT.

5.2.4 RAMAN:

Figure 44 shows the Raman spectra of the PZT Palette sintered at 1200∘C for 4h. The peaks with wave numbers of 138, 197, 274, 334, 544, 606, and 718 cm⁻¹ were assigned to the tetragonal PZT phase [40, 57]. These peaks are identified as A1(1TO), E(2TO), B1+E, A1(2TO), E(3TO), A1(3TO) and E(3LO) +A1(3LO) modes, respectively.
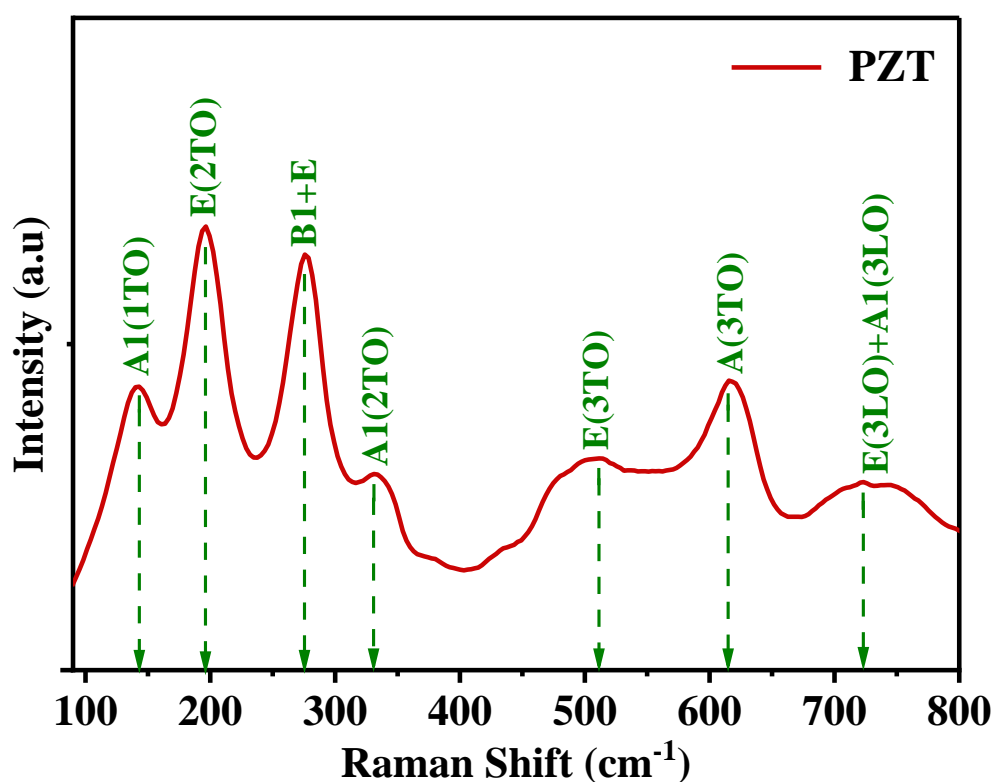

Figure 44 Raman spectra of massicot(β-PbO) and PZT Palette sintered at 1200°C.

Since ancient times, massicot has been utilized as a yellow pigment. It is a very effective Raman scatterer and seems stable within the experimental setup used here. It didn't begin to degrade until it was exposed to 514.5 nm radiation at a very high laser power.

5.3 Dielectric Properties:

Wayne Kerr Precision Impedance analyzer was used to investigate the dependence of Dielectric parameters such as dielectric permittivity, dielectric loss, tangent loss factor, AC conductivity, impedance to frequency. Compacted pallets were prepared and sintered and applied with silver paste for the measurements.

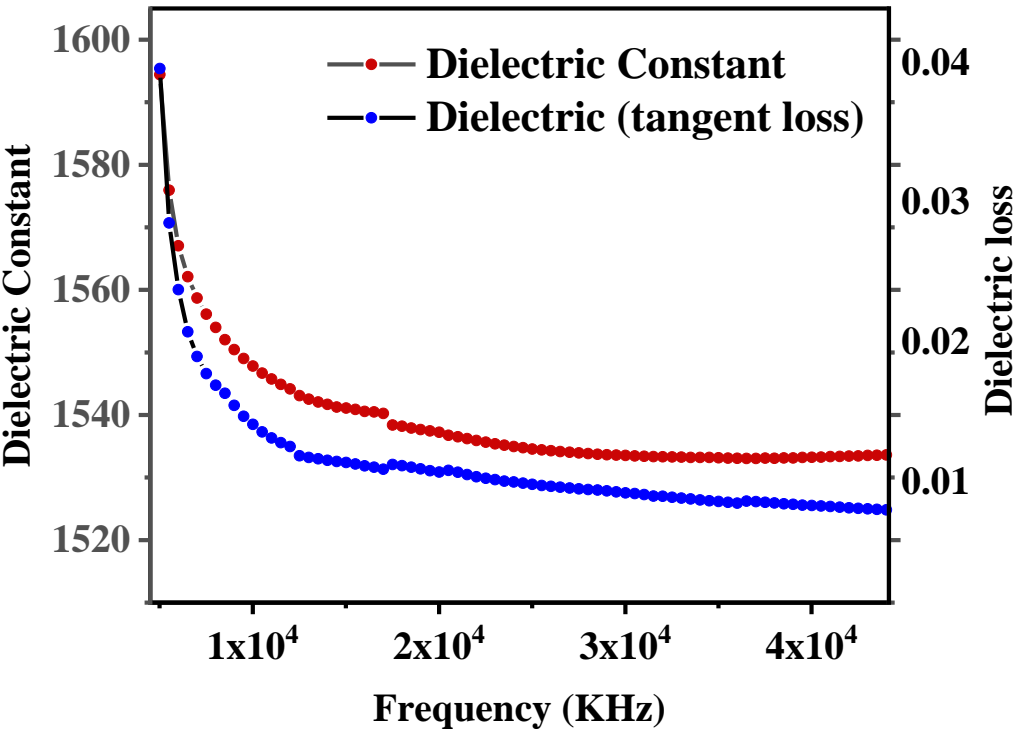### 5.3.1 Dielectric Constant and Tangent loss as Function of Frequency:

Figure 45 Dielectric constant and tangent loss vs Frequency For PZT

It was found that a material's dielectric constant falls as frequency rises. This curve's trend can be described by the Maxwell-Wagner model. Charge building up at the interface of two different materials conductive and nonconductive is explained by the Maxwell-Wagner effect. As a result, the interface accumulates charges in proportion to the applied voltage by preventing the flow of charge from the conducting part into the non-conductive zone. One layer of conducting grains and insulating or less conductive grain boundaries make up the ceramic material's interface. Electrons start travelling to the grain boundaries using the hopping mechanism once an electric field has been applied across the dielectric material. The borders of the grains are resistant. This resistive property causes charge build up and space charge polarization, and collected charge carriers need some time to line up with the external field. Low frequencies make it simpler to maintain this process, which results in higher dielectric permittivity values. Reduced polarization

and dielectric permittivity result from the charge carriers' inability to reach the grain boundaries and align with the external field as frequency rises. The shift of the PZT's dielectric constant (ε) and dielectric loss (tan δ) as a function of frequency is shown in Fig. 45 at room temperature. It has been discovered that when frequency increases, the dielectric constant, and the dielectric loss both drop and exhibit a typical characteristic of normal dielectrics.

5.3.2 Dielectric Loss as Function of Frequency:

The dielectric loss behaves with frequency in a dispersion manner like the dielectric constant. In contrast to ferrites, virtually little dielectric loss occurs. Polarization is a fundamental characteristic of the PZT ferroelectric phase; therefore, this is clear. It may be seen that when frequency increases, dielectric loss generally reduces. Then, as the frequencies grow, the additional dielectric loss fairly remains constant. Lower frequency measurements reveal relatively minor dielectric losses, which may be caused by both space charge polarization and structural inhomogeneity.
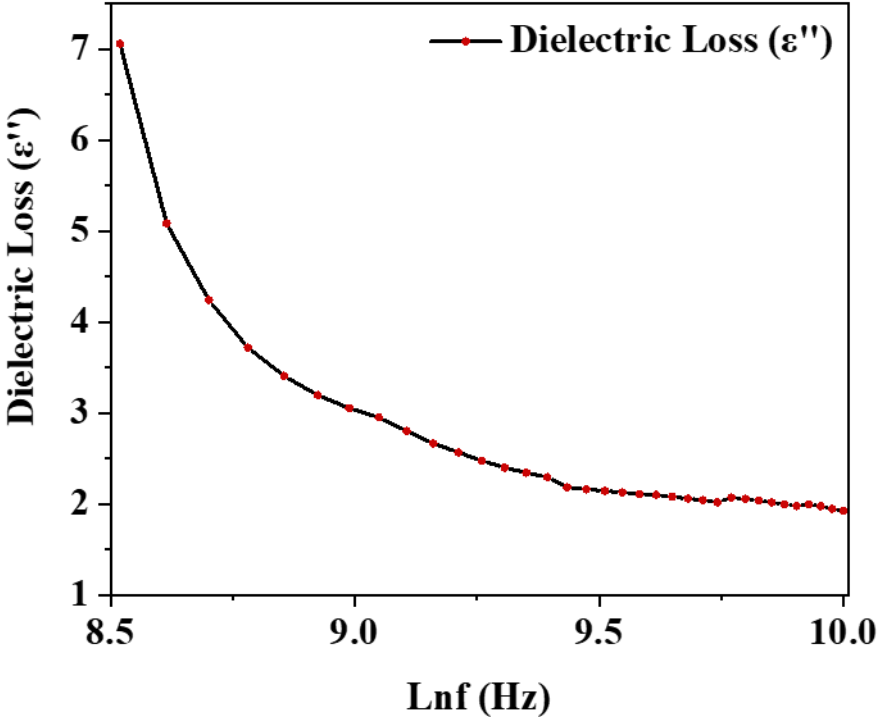

Figure 46 Dielectric loss and vs Frequency For PZT

5.3.3 AC Conductivity:

Further, the ac conductivity of the PZT sample was measured with the frequency figure 47 and it relates to the material's dielectric constant to analyze the conduction mechanism of the as-

prepared PZT sample.
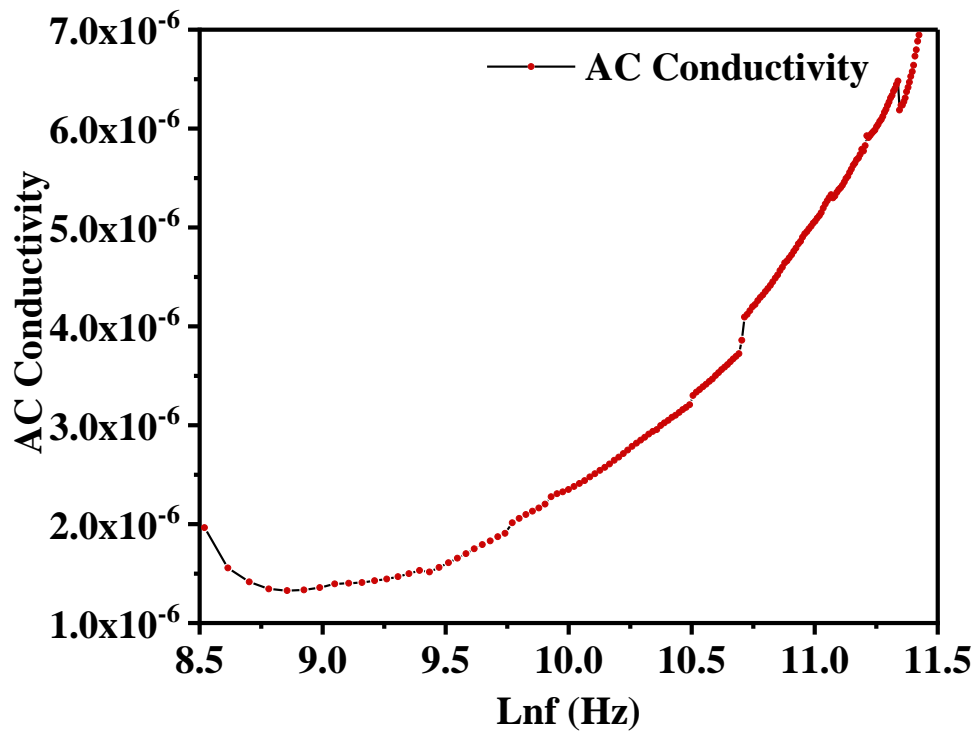
$$\sigma_{ac} = 2\pi f \varepsilon'' \varepsilon_0$$

Figure 47 AC conductivity vs Frequency For PZT

It was shown that the frequency promotes the ac conductivity. Frequency-dependent ac conductivity is due to the charge carriers' hopping process, which increases conductivity as frequency increases. The Koops model may be used to explain why ac increases with frequency[58, 59]. This model predicts that PZT material will have less conductivity at lower frequencies. The development of potential barriers at the grain borders, which prevent the movement of charge carriers from one grain to another, may be the cause of the reduced hopping mechanism that causes the conductivity to drop at lower frequencies. According to the Maxwell-Wagner model, charge carriers behave in this way.

5.3.4 Impedance:

Figure 48 depicts the impedance and frequency curve of PZT ceramics. The overall system resistance is referred to as the system's impedance. The resistance's magnitude (Z') is decreasing as frequency increases. The observation shows that the compounds' ac conductivity increases as frequency increases. Higher frequencies may have resulted in a reduction in the compounds' barrier qualities. Due to the high impedance of the materials, space charges are not responsive to applied electric fields at lower frequencies [60].
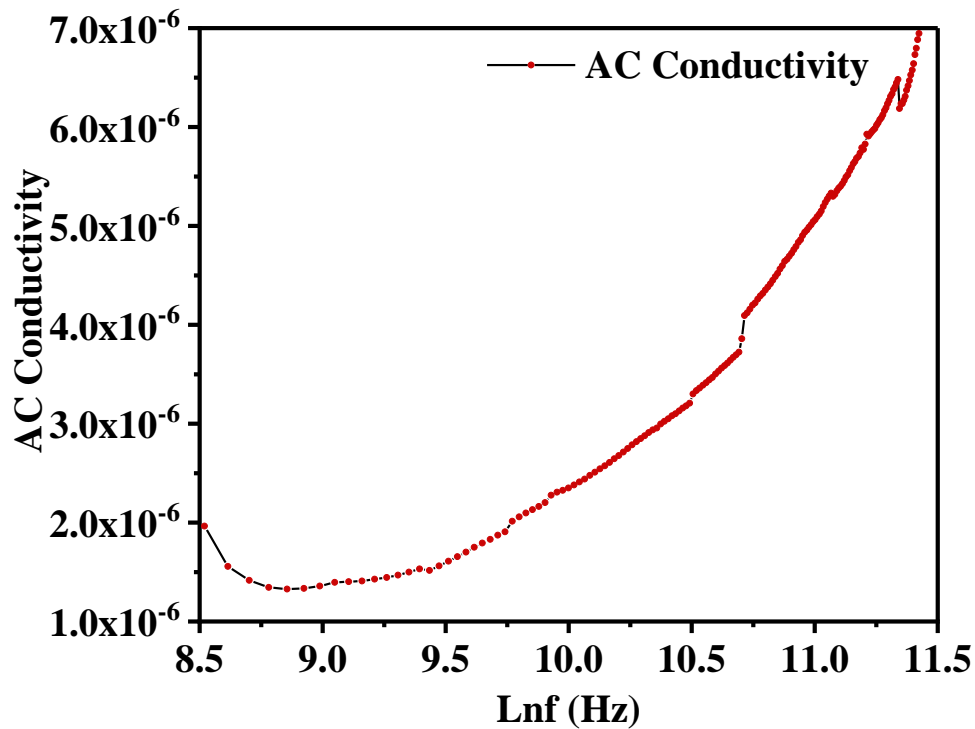
Figure 48 Impedance (real part) and vs Frequency For PZT

5.2 Ferroelectric Characterizations:

5.3.1 Polarization *vs.* Electric Field:

PZT is a particular class of ferroelectric material that comprises domain. An area of a ferroelectric where spontaneous polarization is consistently orientated is known as a ferroelectric domain. Under the influence of a DC electric field, the local spontaneous polarization of the ferroelectric material PZT may be switched between two or more corresponding crystallographic orientations. By applying an electrical field (E) stronger than a coercive field (E_C), ferroelectric ceramics can be rendered piezoelectric (poled) below the Curie temperature (T_C). Saturation polarization (P_{SAT}) is the term for the highest degree of polarization in a ferroelectric material. Domains are oriented in the direction of the applied field by the poling process, producing a net remnant polarization P_r [61]. The primary property of piezoelectric materials is residual polarization. Remaining polarization after the poling field is removed and the coercive field, which is needed to flip half of the previously induced remnant polarization so that the net remnant polarization is zero, are the two characteristics of polarized piezoelectric materials. P-E hysteresis loops can be used to measure polarization. In general, sample pellets were made, sintered at a temperature of 1200°C, poled, and their characteristics were examined. It should be noted that the powder exhibits a typical ferroelectric material loop and saturation polarization of 7.5 µC/cm^2 however there is leakage of current making the pellet unstable at 2000V Fig 49.

58

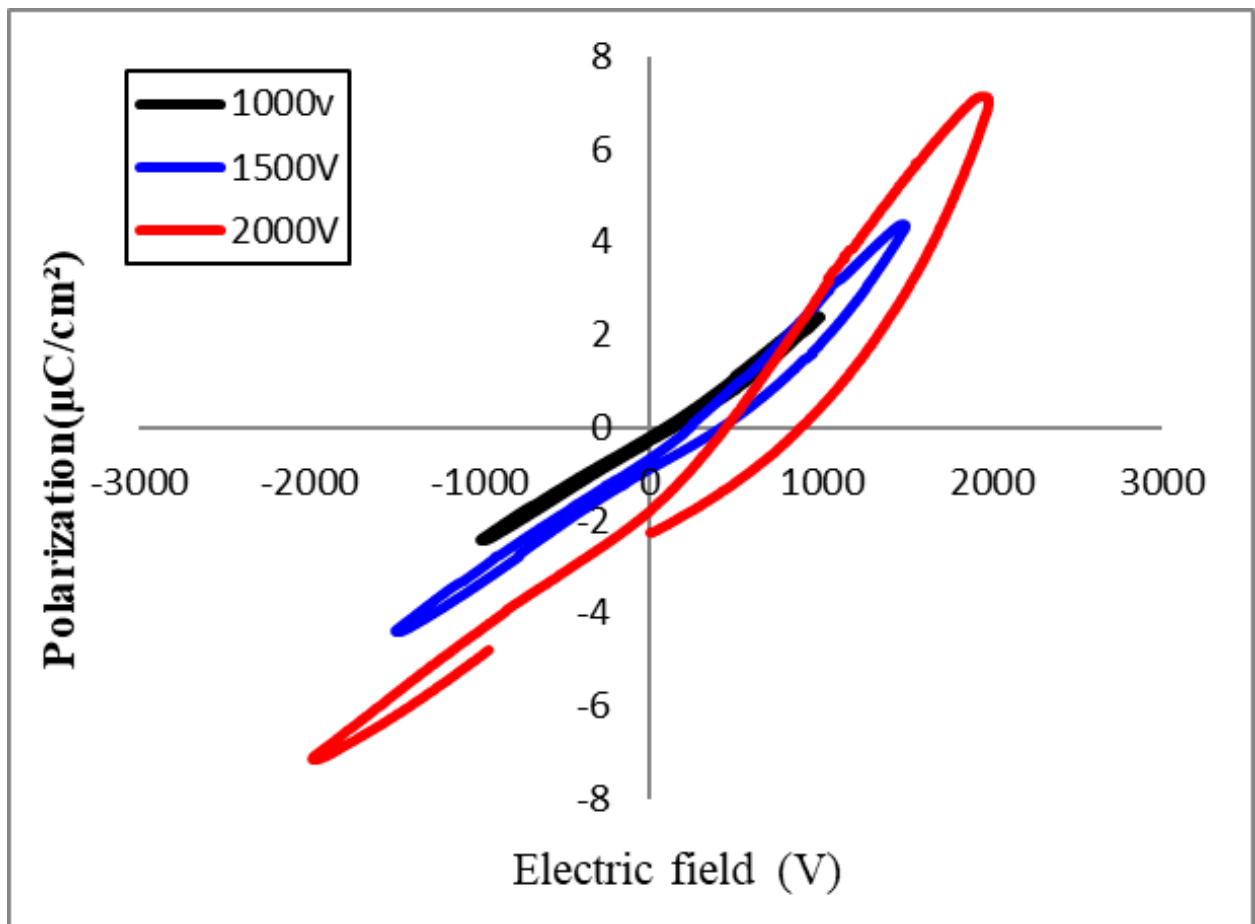Figure 49 Polarization vs electric field P-E loop

Conclusion

In this work we have successfully synthesized $Pb(Zr_{0.52}Ti_{0.48})O_3$ using commercially available precursors. PbO was synthesized using spent lead acid batteries. This method is simple, inexpensive, and economical and was introduced as reproducible process. The XRD analysis indicates that the obtained PbO has the orthorhombic structure which corresponds to β-PbO . PZT ceramics have been fabricated from their oxide mixture via reactive sintering with involving the calcination step, which is necessary in the traditional solid-state reaction process and most of the chemical methods. PZT Sintered at 1200°C has a piezoelectric coefficient d_{33} of 307(pC/N), a Q_m factor of 2081.80, and a dielectric constant of 1597 at 8.5 Hz. Researcher successfully concludes that spent lead acid batteries can be used to synthesize PZT with local available precursors and better dielectric properties. These $Pb (Zr_{0.52}Ti_{0.48})O_3$ have promising application for actuators and sensors.

References

[1]. Jaffe, B., W.R. Cook, and H. Jaffe, *Piezolectric ceramics*. (1971), -.

[2]. Necira, Z., et al., *Synthesis of PZT powder by conventional method at various conditions*. EPJ Web of Conferences, (2012). **29**: p. 00038.

[3]. Ren, L., X. Luo, and H. Zhou, *The tape casting process for manufacturing low-temperature co-fired ceramic green sheets: A review*. Journal of the American Ceramic Society, (2018). **101**(9): p. 3874-3889.

[4]. Shirane, G., K. Suzuki, and A. Takeda, *Phase Transitions in Solid Solutions of PbZrO3 and PbTiO3 (II) X-ray Study*. Journal of the Physical Society of Japan, (1952). **7**(1): p. 12-18.

[5]. Rodel, J., et al., *Perspective on the Development of Lead-Free Piezoceramics*. Journal of the American Ceramic Society, (2009). **92**.

[6]. Rödel, J., et al., *Transferring lead-free piezoelectric ceramics into application*. Journal of the European Ceramic Society, (2015). **35**(6): p. 1659-1681.

[7]. Britain, G., *The Restriction of the Use of Certain Hazardous Substances in Electrical and Electronic Equipment Regulations 2012*. (2012): Stationery Office.

[8]. Curie, J. and P. Curie. *Développement par compression de l'électricité polaire dans les cristaux hémièdres à faces inclinées*.

[9]. wu, A., et al., *Sol–Gel Preparation of Lead Zirconate Titanate Powders and Ceramics: Effect of Alkoxide Stabilizers and Lead Precursors*. Journal of the American Ceramic Society, (2000). **83**: p. 1379.

[10]. Finger, L.W., *Physical Properties of Crystals, Their Representation by Tensors and Matrices*. Eos, Transactions American Geophysical Union, (1983). **64**(45): p. 643-643.

[11]. Keve, E.T. and K.L. Bye, *Phase identification and domain structure in PLZT ceramics*. Journal of Applied Physics, (1975). **46**(2): p. 810-818.

[12]. HAERTLING, G.H. and C.E. LAND, *Hot-Pressed (Pb,La)(Zr,Ti)O3 Ferroelectric Ceramics for Electrooptic Applications*. Journal of the American Ceramic Society, (1971). **54**(1): p. 1-11.

[13]. Bobnar, V., Z. Kutnjak, and A. Levstik, *Glassy to inhomogeneous-ferroelectric crossover in (Pb,La)(Zr,Ti)O3 ceramics*. Applied Physics Letters, (2000). **76**(19): p. 2773-2775.

[14]. Gao, X., et al., *Piezoelectric Actuators and Motors: Materials, Designs, and Applications*. Advanced Materials Technologies, (2020). **5**(1): p. 1900716.

[15]. Sharma, L.K., et al., *A Case Study of Improving Yield Prediction and Sulfur Deficiency Detection Using Optical Sensors and Relationship of Historical Potato Yield with Weather Data in Maine.* Sensors, (2017). **17**(5): p. 1095.

[16]. Wu, J., D. Xiao, and J. Zhu, *Potassium–Sodium Niobate Lead-Free Piezoelectric Materials: Past, Present, and Future of Phase Boundaries.* Chemical Reviews, (2015). **115**(7): p. 2559-2595.

[17]. Wu, J., *Perovskite lead-free piezoelectric ceramics.* Journal of Applied Physics, (2020). **127**(19): p. 190901.

[18]. Maeder, M.D., D. Damjanovic, and N. Setter, *Lead Free Piezoelectric Materials.* Journal of Electroceramics, (2004). **13**(1): p. 385-392.

[19]. Lines, M.E., *Principles and applications of ferroelectrics and related materials / by M. E. Lines and A. M. Glass.* The International series of monographs on physics, ed. A.M. Glass. (1977), Oxford [Eng.]: Clarendon Press.

[20]. Nelmes, R.J., et al., *Order-disorder behaviour in the transition of PbTiO3.* Ferroelectrics, (1990). **108**(1): p. 165-170.

[21]. Meštrić, H., et al., *Iron-oxygen vacancy defect centers in $\mathrm{Pb}\mathrm{Ti}{\mathrm{O}}_{3}$: Newman superposition model analysis and density functional calculations.* Physical Review B, (2005). **71**(13): p. 134109.

[22]. Glazer, A.M. and S.A. Mabud, *Powder profile refinement of lead zirconate titanate at several temperatures. II. Pure PbTiO3.* Acta Crystallographica Section B, (1978). **34**(4): p. 1065-1070.

[23]. Harada, J., T. Pedersen, and Z. Barnea, *X-ray and neutron diffraction study of tetragonal barium titanate.* Acta Crystallographica Section A, (1970). **26**: p. 336-344.

[24]. Cohen, R.E., *Origin of ferroelectricity in perovskite oxides.* Nature, (1992). **358**: p. 136-138.

[25]. Noheda, B., et al., *A monoclinic ferroelectric phase in the Pb(Zr1−xTix)O3 solid solution.* Applied Physics Letters, (1999). **74**(14): p. 2059-2061.

[26]. Sawaguchi, E., *Ferroelectricity versus Antiferroelectricity in the Solid Solutions of PbZrO3 and PbTiO3.* Journal of the Physical Society of Japan, (1953). **8**(5): p. 615-629.

[27]. Jaffe, B., R.S. Roth, and S. Marzullo, *Piezoelectric Properties of Lead Zirconate-Lead Titanate Solid-Solution Ceramics.* Journal of Applied Physics, (1954). **25**(6): p. 809-810.

[28]. Isupov, V.A., *Phases in the PZT Ceramics.* Ferroelectrics, (2002). **266**(1): p. 91-102.

[29]. Haertling, G.H., *Ferroelectric Ceramics: History and Technology.* Journal of the American Ceramic Society, (1999). **82**(4): p. 797-818.

[30]. Uchino, K., *Ferroelectric devices.* (2018): CRC press.

[31]. Zhou, D., M. Kamlah, and D. Munz, *Effects of Bias Electric Fields on the Non-linear Ferroelastic Behavior of Soft Lead Zirconate Titanate Piezoceramics.* Journal of the American Ceramic Society, (2005). **88**(4): p. 867-874.

[32]. Su, B., C.B. Ponton, and T.W. Button, *Hydrothermal and electrophoretic deposition of lead zirconate titanate (PZT) films.* Journal of the European Ceramic Society, (2001). **21**(10): p. 1539-1542.

[33]. Lal, R., R. Krishnan, and P. Ramakrishnan, *Preparation and characterization of submicron reactive PZT powders.* Materials Science and Engineering, (1987). **96**(C): p. L25-L29.

[34]. Singh, A.P., et al., *Low-temperature synthesis of chemically homogeneous lead zirconate titanate (PZT) powders by a semi-wet method.* Journal of Materials Science, (1993). **28**(18): p. 5050-5055.

[35]. Buchanan, R.C. and J. Boy, *Effect of Powder Characteristics on Microstructure and Properties in Alkoxide-Prepared PZT Ceramics.* Journal of The Electrochemical Society,(1985). **132**(7): p. 1671.

[36]. Branković, Z., et al., *Mechanochemical synthesis of PZT powders.* Materials Science and Engineering A, (2003). **345**(1-2): p. 243-248.

[37]. Wang, S.F., et al., *Characterization of hydrothermally synthesized lead zirconate titanate (PZT) ceramics.* Materials Chemistry and Physics, (2004). **87**(1): p. 53-58.

[38]. Bortolani, F. and R.A. Dorey, *Synthesis of spherical lead zirconate titanate (PZT) nanoparticles by electrohydrodynamic atomisation.* Advances in Applied Ceramics, (2009). **108**(6): p. 332-337.

[39]. Bortolani, F. and R.A. Dorey, *Molten salt synthesis of PZT powder for direct write inks.* Journal of the European Ceramic Society, (2010). **30**(10): p. 2073-2079.

[40]. Mu, G., et al., *Synthesis of PZT nanocrystalline powder by a modified sol–gel process using water as primary solvent source.* Journal of Materials Processing Technology, (2007). **182**(1): p. 382-386.

[41]. Aksel, E. and J.L. Jones, *Advances in Lead-Free Piezoelectric Materials for Sensors and Actuators.* Sensors, (2010). **10**(3): p. 1935-1954.

[42]. Hiruma, Y., H. Nagata, and T. Takenaka, *Phase diagrams and electrical properties of (Bi1/2Na1/2)TiO3-based solid solutions.* Journal of Applied Physics, (2008). **104**(12).

[43]. EGERTON, L. and D.M. DILLON, *Piezoelectric and Dielectric Properties of Ceramics in the System Potassium—Sodium Niobate.* Journal of the American Ceramic Society, (1959). **42**(9): p. 438-442.

[44]. de Oliveira, C. and T. Werlang, *Ergodic hypothesis in classical statistical mechanics.* Revista Brasileira de Ensino de Física, (2007). **29**: p. 189-201.

[45]. Morita, T., *Piezoelectric Materials Synthesized by the Hydrothermal Method and Their Applications.* Materials, (2010). **3**.

[46]. Zhu, M., et al., *Lead-Free (K0.5Bi0.5)TiO3 Powders and Ceramics Prepared by a sol–Gel Method.* Materials Chemistry and Physics - MATER CHEM PHYS, (2006). **99**: p. 329-332.

[47]. Rödel, J., et al., *Perspective on the Development of Lead-free Piezoceramics.* Journal of the American Ceramic Society, (2009). **92**(6): p. 1153-1177.

[48]. Sharma, R., et al., *X-ray diffraction: A powerful method of characterizing nanomaterials.* Recent Res. Sci. Tech., (2012). **4**: p. 77-79.

[49]. Melo, R.S., et al., *Magnetic ferrites synthesised using the microwave-hydrothermal method.* Journal of Magnetism and Magnetic Materials, (2015). **381**: p. 109-115.

[50]. Stuart, B.H., *Infrared Spectroscopy: Fundamentals and Applications.* (2004): J. Wiley.

[51]. Verma, R., *Introduction to Fourier Transform Infrared Spectrometry.* (2022).

[52]. Alagar, M., T. Thirugnanasambandan, and A. Raja, *Chemical Synthesis of Nano-Sized particles of Lead Oxide and their Characterization Studies.* Journal of Applied Sciences, (2012). **12**.

[53]. Bell, I.M., R.J.H. Clark, and P.J. Gibbs, *Raman spectroscopic library of natural and synthetic pigments (pre- ≈ 1850 AD).* Spectrochimica Acta Part A: Molecular and Biomolecular Spectroscopy, (1997). **53**(12): p. 2159-2179.

[54]. Srivastava, G. and V. Tiwari, *Structural, dielectric and piezoelectric properties of 0–3 PZT/PVDF composites.* Ceramic International, (2015). **41**.

[55]. Zhang, D.-Q., et al., *Structural and Electrical Properties of PZT/PVDF Piezoelectric Nanocomposites Prepared by Cold-Press and Hot-Press Routes.* Chinese Physics Letters, (2008). **25**: p. 4410.

[56]. Akimov, A.I., G.K. Savchuk, and T.M. Akimova, *Vibrations of the Crystal Lattice of Solid Solutions of Lead Zirconate-Titanate.* Journal of Applied Spectroscopy, (2003). **70**: p. 498-502.

[57]. Burns, G. and B.A. Scott, *Raman Spectra of Polycrystalline Solids; Application to the $\mathrm{Pb}{\mathrm{Ti}}_{1\ensuremath{-}x}{\mathrm{Zr}}_{x}{\mathrm{O}}_{3}$ System.* Physical Review Letters, (1970). **25**(17): p. 1191-1194.

[58]. Koops, C.G., *On the Dispersion of Resistivity and Dielectric Constant of Some Semiconductors at Audiofrequencies.* Physical Review, (1951). **83**(1): p. 121-124.

[59]. Kharabe, R.G., et al., *Dielectric properties of mixed Li–Ni–Cd ferrites.* Smart Materials and Structures, (2006). **15**(2): p. N36.

[60]. Sebastian, M.T., *Dielectric materials for wireless communication.* (2010): Elsevier.

[61]. Haider, M.F., et al., *Characterization of Piezo Electric Wafer Active Sensors After Exposure to High Temperature.* (2016). V06AT06A016.